β-mercaptoethanol in 500 mM Tris HCl, pH 6.8), boiled at 100°C for 5 min; centrifuged, and the supernatant analyzed by SDS-PAGE.

Heme peroxidase activity based heme-binding assay

Binding assay based on the peroxidase activity of bound heme was performed as detailed by [38,39]. Briefly, micro-titer plate coated with serial dilutions of the recombinant protein was incubated with hemin (20 µg/100 µl) at 37°C for 1 h. The unbound hemin was removed and the wells were washed three times with PBS (pH 7.3). 50 µl of ready-to-use substrate tetramethylbenzidine/H_2O_2 (TMB) (Bangalore-Genei, India) was added and the reaction stopped after 15 min with addition of equal volume of 1N H_2SO_4. The OD_{450} was determined in an ELISA plate reader (Bio-Rad, USA). The amount of hemin bound to protein was calculated from a linear graph of the peroxidase activities of known concentrations of hemin.

Heme spectrometric titration

Optical absorption spectrometric studies were performed on Hitachi U-3900H spectrophotometer according to method detailed by [40]. Briefly, the binding of proteins to heme was titrated by adding increasing amount of the protein (0–28 µM) to 10 µM of heme in 40% dimethyl sulfoxide (DMSO) buffered with 20 mM HEPES (pH 7.4). Difference in absorption spectra over a range of 350 to 700 nm was recorded. We used the increase in absorbance at Soret peak (412 nm) to monitor the formation of the protein heme complex. The heme binding curve was constructed by plotting the change in absorbance at the Soret peak (ΔA_{412}) versus the protein concentrations. The heme-binding curve was fitted using *one site specific binding with Hill slope* model on GraphPad Prism, v5.00.

Statistics

Data analysis was performed on GraphPad Prism, v5.00. Mann-Whitney test was used to compare differences between two groups, while Kruskal-Wallis test was applied to compare differences among several groups. All plotted data are means with error bars representing standard deviation (SD). Statistical significance was designated as $p<0.05$.

Accession numbers

PFAM: PF01390, SCOP: 82671, SCOP: 54861, PDB: 2e7v, PDB: 2acm, PDB: 1ivz, GenBank: AY570748, GenBank: AY570737, GenBank: AY570742.

Results

Molecular structure model based identification of extracellular SEA-domain

We had identified a novel gene family with similar signal sequence and promoter regions among SST isolated cDNAs (Figure S1A) [26], and showed that this gene family had originated from retrotransposon-mediated gene duplication mechanism [27]. Although several transcripts from ~27 duplicons were found to belong to this family, we could not readily identify the molecular functions of these genes since no sequence homolog was readily identifiable in any other organism [27]. Consequently, we utilized comparative structural homology modeling to identify features and domains that could predict the putative molecular functions of the encoded proteins. Firstly, protein topology indicated that while all the members of this family bear similar signal sequence and are thus trafficked to the surface; some also contain C-terminal transmembrane regions, akin to type-I transmembrane proteins (Figure S1B).

The molecular folding patterns of the proteins were modeled simultaneously in *Phyre* 2 and *Rosetta* using fold recognition and *ab-initio* structure predictions (Figure S1C). These programs create sequence alignment profiles from PSI-Blasts followed by scanning of 'fold library' to identify remote structural homologs from experimentally determined structures in PDB and SCOP databases [33,34]. The secondary structure components showed antiparallel arrangement of β-sheets, backed by α-helices (Figure 1A), typical of ferredoxin-like folds. Interestingly, models from both programs identified an extracellular domain of ~120 amino acids common among this family, with striking similar folding pattern as SEA-domain (**s**ea urchin protein, **e**nterokinase and **a**grin) [PFAM: PF01390; SCOP: 82671] (Figure 1A and Table S1). SEA-domain is a domain with ferredoxin-like fold [SCOP: 54861], found in several proteins of diverse functions in different organisms [28–30,41,42]. Notably, crystal structure of the SEA-domain of transmembrane protease serine II (TMPRSS2) of *Mus musculus* [PDB: 2e7v] was the highest scoring template at over 95% confidence, according to which the shown structures were modeled. For clarity, only the original SST identified candidates are shown as representative of the family (Figure 1A). The structural models for all members of the gene family are summarized in Table S1. Other high scoring homologs at over 95% precision were the SEA-domains of Mucin 1 [PDB: 2acm] and Mucin 16 [PDB: 1ivz].

To validate the models, rigid body superposition with the highest scoring template [PDB: 2e7v] was performed. The result showed Cα and main chain root mean square deviations (RMSD) of 0.680 Å and 0.838 Å respectively for SjCP3842, a representative member of this gene family (Figure 1B). Similar low RMSD values were recorded for the other candidates. Ramachandran plot (ϕ/ψ) of conformation angles for each residue showed over 98% of the residues in the favored region, with less than 2% in the outlier region. These results indicate the reliability of the predicted models (Figure 1B).

A reciprocal *'BackPhyre'* using the modeled structures to scan over 25 genomes also mapped the domain to SEA-domains at over 95% confidence, albeit with limited protein sequence homology. The low sequence similarity (Figure 1C) observed from alignments of this extracellular domain with two major SEA-domains (MUC1 and TMPRSS2) could imply that this structural similarity is at least partly independent of amino acid sequence homology [29]. As a matter of fact, SEA-domains are primarily defined by their characteristic folding pattern, extracellular localization on transmembrane proteins, their ability to assist or regulate binding to glycans, and their presence in proteins with *O*-linked glycans [28,29,41]. As expected, multiple *O*-glycosylation sites were identified by posttranslational modification prediction. We also confirmed that the expressed proteins contain *O*-linked glycans using glycoprotein detection assay (Figure S2). Equally, two conserved cysteine residues are present in all the candidates (Figure S1A), which could be structurally important by providing disulfide bridges in the folded protein.

Further evidence to classify the identified domain as SEA-module was the identification of the typical glycine-serine amino acid consensus (FRPG/SVVV) [30] auto-cleavage site of SEA-domains (Figure 1C). Some SEA-domain proteins have been shown to undergo auto-cleavage, although the resulting subunits remain non-covalently associated in the native state [30,41,42]. This cleavage site is usually located within the bend between β2 and β3 sheets [30] as we equally observed (red arrow in Figure 1 A and C). In addition, the SDS fractionated recombinant protein

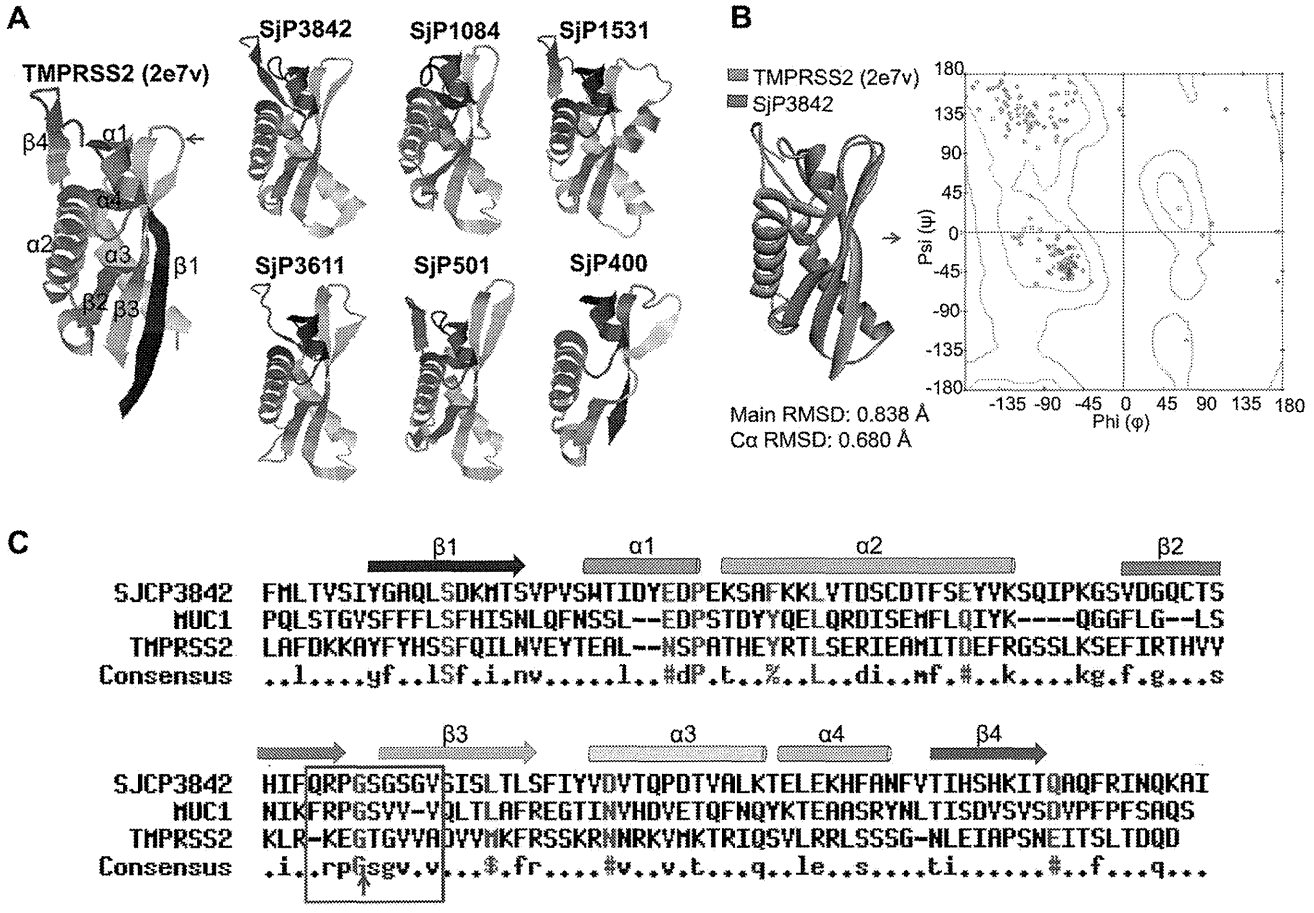

Figure 1. Extracellular loop of the candidate proteins contain SEA-domains. (**A**) Modeled molecular structures of the extracellular domains with striking similarity with SEA-domain. Also shown for comparison is the SEA-domain of mouse TMPRSS2. Typical of SEA-domains, the secondary structure components showed an antiparallel arrangement of β-sheets. A summary of structural models of the entire transcripts in this gene family is shown in Table S1. (**B**) Rigid body superposition of SjP3842 (blue) over the highest scoring template, PDB: 2e7v (olive). The graph is the Ramachandran plot (ϕ/ψ) showing conformational angles distribution of the residues. Over 98% of residues were in the favored regions while less than 2% were in the outlier region. (**C**) Alignments of SjCP3842 with two well defined SEA-domains (human MUC1 and mouse TMPRSS2). Putative SEA-domain consensus cleavage site (red arrow) was identified between β2 and β3.
doi:10.1371/journal.pntd.0002644.g001

(shown later) contained extra bands of expected molecular weight as the potential cleavage products. Taken together, these results provide multiple grounds to classify this extracellular domain as SEA-domain.

Identification of heme-binding site on the SEA-domain

To provide lead to the possible molecular function of the gene products, we subjected the modeled structures to ligand binding site identification using *3DLigandSite* [35]. This program uses protein structure to search a structural library to identify homologous structures with bound ligands, which are then superimposed on the protein structure to predict potential ligand binding sites [35]. Interestingly, a binding site was observed for Fe-protoporphyrin-IX (heme) at significantly high precision (Figure S3). Binding sites for energy transfer coenzymes including ATP, and several metal ions (Mg, Zn, Cu) binding sites were also identified. The heme-binding site was predicted based on 178 heme ligands present in 177 homologous structures with bound heme (Figure S3).

Analysis of the modeled heme-binding pocket of SjCP3842 showed that the vinyl end of the amphiphilic heme is inserted into a hydrophobic cavity created between α2 and α3 helices, and β2 and β3 sheets (Figure 2 A and B). Many of the interacting residues in the binding pocket are conserved among the members of this protein family (labeled in red in Figure S4B), consistent with binding of a heme group. The hydrophilic propionate end (red sphere) of heme is rather facing away from the hydrophobic pocket (Figure 2 A and B), with one propionate group engaged in electrostatic interactions with a nitrogen atom in Arg-157 side chain (Figure 2C). The phenyl rings of three conserved phenyl-alanine residues (Phe-80, Phe-140 and Phe-156) and one other phenylalanine (Phe-143) engage in pi-stacking interactions with the heme Pyrrole rings, which further stabilize heme-binding (Figure S4B). There were also polar contacts between heme and Thr-79, Tyr-83, His-147 and His-149 (Figure S4B), and several hydrogen bond interactions within the binding site.

Consistent with binding to heme, we readily identified potential axial ligands for heme iron, indicating hexa-coordination state involving two possible pairs. The imidazole group on His-149 side chain (bond distance of 2.0 Å) is the putative proximal ligand with either His-147 (Figure 2C) or the thioether group on Met-50 (Figure S4C) as the distal ligand of heme iron. However, the exact pair of axial ligands or the possibility of simultaneously binding two molecules of heme needs to be experimentally clarified.

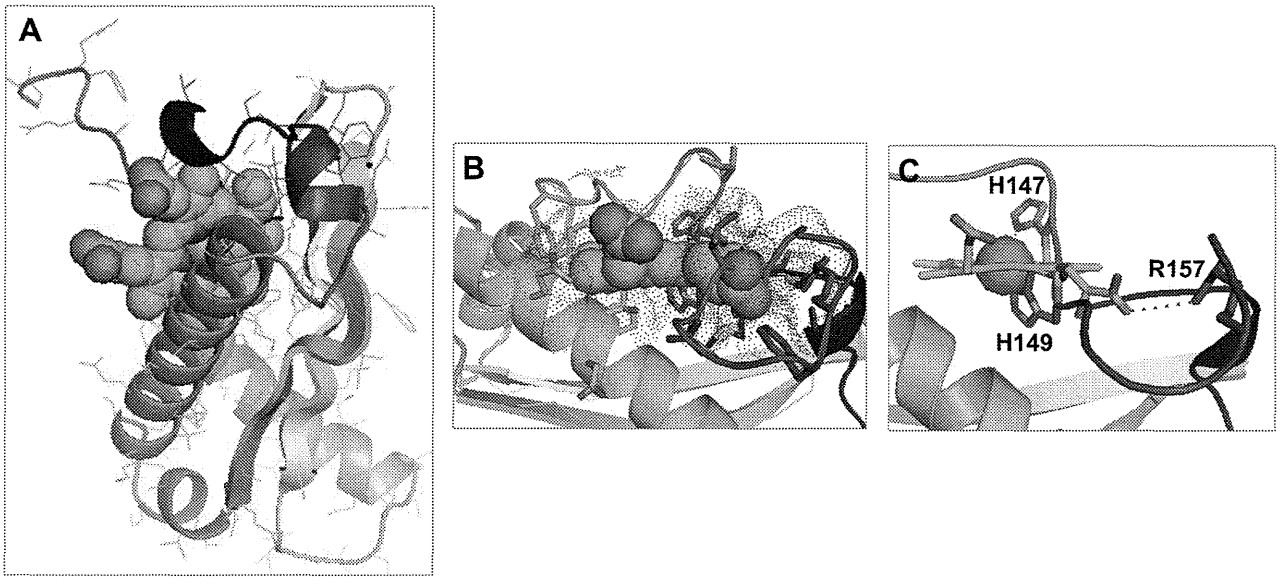

Figure 2. Heme-binding pocket of SjCP3842. (**A**) Heme-binding mode of SjCP3842 showing the hydrophobic vinyl end of the protoporphyrin heme inserted into a hydrophobic cavity, while hydrophilic propionate end of points away from the pocket. Heme is represented using spheres model colored by atoms (C: green, N: blue, O: red, Fe: brown). The protein is shown using cartoon model. (**B**) Heme-binding site showing the Connolly surface of the binding pocket (dots). (**C**) Heme iron (brown sphere) hexa-coordinated with His-149 and His-147 as axial ligands.
doi:10.1371/journal.pntd.0002644.g002

Similar binding site characteristics were observed in another characterized candidate (SjCP1531). However, the iron is coordinated to Tyr-154 as its axial ligand (Figure S5).

Developmental stage specific expression of the candidate genes

We investigated whether this gene family is differentially expressed among developmental stages of *S. japonicum* by stage specific mRNA expression using real time PCR. All other *in-vitro* based characterization was limited to three candidates: SjCP3842 [GenBank: AY570748], SjCP1084 [GenBank: AY570737] and SjCP1531 [GenBank: AY570742]. Relative expression of each candidate gene was quantified and expressed as copy number per nanogram of cDNA (Figure 3 and Table S2). There was differential expression of the three genes among developmental stages of the parasite, with SjCP3842 expressed at higher levels relative to the other two characterized candidates (Figure 3 and Table S2). SjCP3842 was overtly expressed in the adult stage (5680±370.9), although at a higher level in female adult worm (4846±302.1) as compared to the male worms (2000±453.9). The expression levels in the snail intermediate inhabiting sporocyst (2474±627.2) and infective cercaria (2871±98.4) stages were also relatively high as compared to somula (543.4±64.1) and egg stage (252±370.1). SjCP3842 was expressed at the minimal level in the egg stage (Figure 3A). Conversely, SjCP1084 was mainly expressed in the egg stage in relation to other stages. However, the expression levels of SjCP1531 in all stages of the parasite were relatively low and mainly expressed at the egg and adult stages (Figure 3C and Table S2).

Cloning, recombinant expression and antigenicity of the candidates

To confirm expression at protein level, we expressed recombinant proteins, generated and used specific immune sera to identify the native proteins in parasite crude extracts. The complete coding regions of the genes were amplified from *S. japonicum* adult worm cDNA library and cloned into the expression vector, pcDNA4-HisMax. For recombinant protein expression, the plasmid constructs were transformed into Freestyle 293 and BL21 *E. coli* cells. The recombinant proteins used for biochemical assays were expressed in Freestyle 293 cells to ensure proper folding and post translational modification. The proteins were found to exist as oligomers in the native state as seen in the multiple bands of additive ~30 kDa subunits observed both on SDS-PAGE (Figure 4A), western blots probed with anti-HisG antibody (Figure 4 B and C), and by multiple peaks from size exclusion chromatography fractions (Figure 4D), all showing the tetramer as the native state. Similar oligomeric state was also predicted by structural modeling (Figure S1D). Oligomerization may have been mediated by the disulfide bridges on two conserved cysteine residues common among the members of this family (Figure S1A). Other extra bands are of same molecular weight as the expected SEA-domain auto-cleavage products (Figure 1C).

To confirm native expression and to show potential antigenicity of the candidates during schistosomiasis, immunoblotting and ELISA techniques were applied. Parasite egg (SEA) and adult worm (SWA) crude antigen preparations were blotted and probed with the polyclonal immune sera (α-SjCP3842, α-SjCP1531 and α-SjCP1084). Blotted protein fractions of sizes similar to both the subunits (~30 kDa) and tetramer (~120 kDa) reacted specifically with the immune sera (Figure 4E). Also, the recombinant proteins specifically reacted with sera from *S. japonicum* infected miniature pigs, with significantly high titers of IgG in ELISA (Figure 4F). These results indicate that this gene family is actually expressed in the parasite, appear functional and potentially antigenic during schistosomiasis.

SEA-domains of *S. japonicum* assist binding to glycosaminoglycans (GAGs)

In addition to their characteristic folding pattern, SEA-domains are known to assist or regulate binding to carbohydrate moieties. We assessed interactions of the characterized SEA-domain

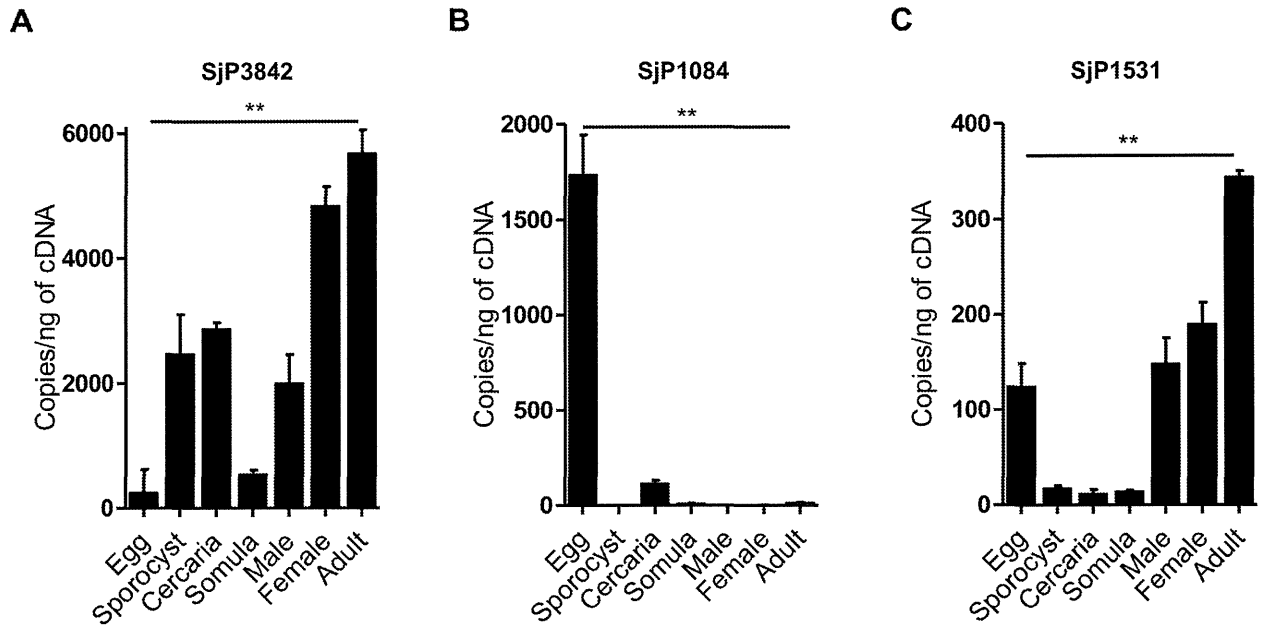

Figure 3. Developmental stage specific expression profiles of the candidate genes. Developmental stage specific expression of the candidate genes presented as copy number per nanogram of cDNA. The full data statistics is shown in a supplementary table (Table S2). There was differential expression of the three characterized genes among developmental stages of the parasite, with SjCP3842 expressed at higher levels relative to the other two candidates. (**A**) SjCP3842 was overtly expressed at the adult stage especially in female adult worm. The expression level at the snail intermediate sporocyst and cercaria stages were also relatively high as compared to schistosomula and egg stage. SjCP3842 was expressed at the minimal level at the egg stage. (B) Conversely, SjCP1084 was mainly expressed at the egg stage in relation to other stages. (C) The expression levels of SjCP1531 in all stages of the parasite were relatively low and mainly expressed at the egg and adult stages. Bars represent standard deviation (SD). * = $p<0.05$, ** = $p<0.01$. n = 4 for each group.
doi:10.1371/journal.pntd.0002644.g003

proteins with glycans using recombinant proteins and array type sugar chips in a Surface Plasmon Resonance (SPR) system [37]. The SPR signal (expressed in resonance units, RU) is proportional to the amount of protein analytes bound to the sugar chains immobilized on the sensor chip in a 48 glycans array. The SPR imaging showed specific binding to sulfated GAGs with relatively high affinity. There was disproportionately high specific binding to chondroitin sulfate, dermatan sulfate (CS-B), heparin, dextran sulfate and other sulfated GAGs (Figure 5). SjCP1084 and SjCP1531 have similar glycan binding pattern while SjCP3842 showed relatively less glycan binding capacity but also preferentially binds sulfated GAGs (Figure 5).

We further confirmed the specificity and affinity of protein-GAG interactions by using chondroitin sulfate GAG (CS-GAG) chip containing all possible sulfated disaccharides subunits of chondroitin sulfate, and different concentrations of the protein as analytes. The glycan array format of the CS-GAG chip used and the SPR imaging of the glycan binding assays are shown in a supplementary file (Figure S6 A and B). The binding kinetics of the carbohydrate-protein interactions showed significant binding affinity to CS-GAGs, with dissociation constant (K_D) within the range of receptor-ligand interactions (Figure S6 C and D). Figure S6C shows the detailed sensorgram and the binding curve of the interaction between SjCP1084 and chondroitin sulfate E ($K_D = 9.84 \times 10^{-9}$ M), as representative of the binding kinetics data. The other K_D values for the interactions of SjCP1084 and SjCP1531 with different sulfated disaccharides of chondroitin sulfate are summarized in Figure S6D, showing values within nanomolar range. These results indicate the specificity and affinity of the observed protein-glycan interactions.

Heme-binding properties of *S. japonicum* SEA-domain proteins

To validate the structure based heme-binding model, we showed heme-binding properties of this family *in-vitro*, by three independent methods: hemin-agarose binding assay, heme-dependent peroxidase activity of protein-hemin complexes and optical UV absorption spectroscopy. First, we showed using SjCP3842 that the purified recombinant protein has potential to bind heme on hemin-agarose beads. The eluted fraction showed evidence of specific binding of the protein to heme (Figure 6A). Same experiment performed using unconjugated Sepharose 4B as negative control did not show any trace of the protein in the eluted fraction. Heme binding assay was repeated using the three characterized candidates and similar specific binding was consistently observed after immunoblotting using immune sera (Figure 6B).

To confirm this observation in the native state, hemin-agarose beads were incubated with parasite adult worm crude antigen (SWA) to isolate the total heme-binding protein fractions in the parasite. The fractions were blotted and probed with monoclonal antibody against SjCP3842 (Figure 6C). The result clearly showed the presence of the protein in the parasite heme-binding protein fractions. The multiple bands are expected molecular weights of the monomer, dimer and tetramer. The fact that binding was ablated by the reducing effect of β-mercaptoethanol and denaturing effect of sodium dodecyl sulfate (SDS) used for elution suggests that the observed heme-binding property is at least partly non-covalently mediated by structure of the folded proteins.

To estimate the amount of heme bound by the protein, we assayed the heme-dependent peroxidase activity of the protein-hemin complex

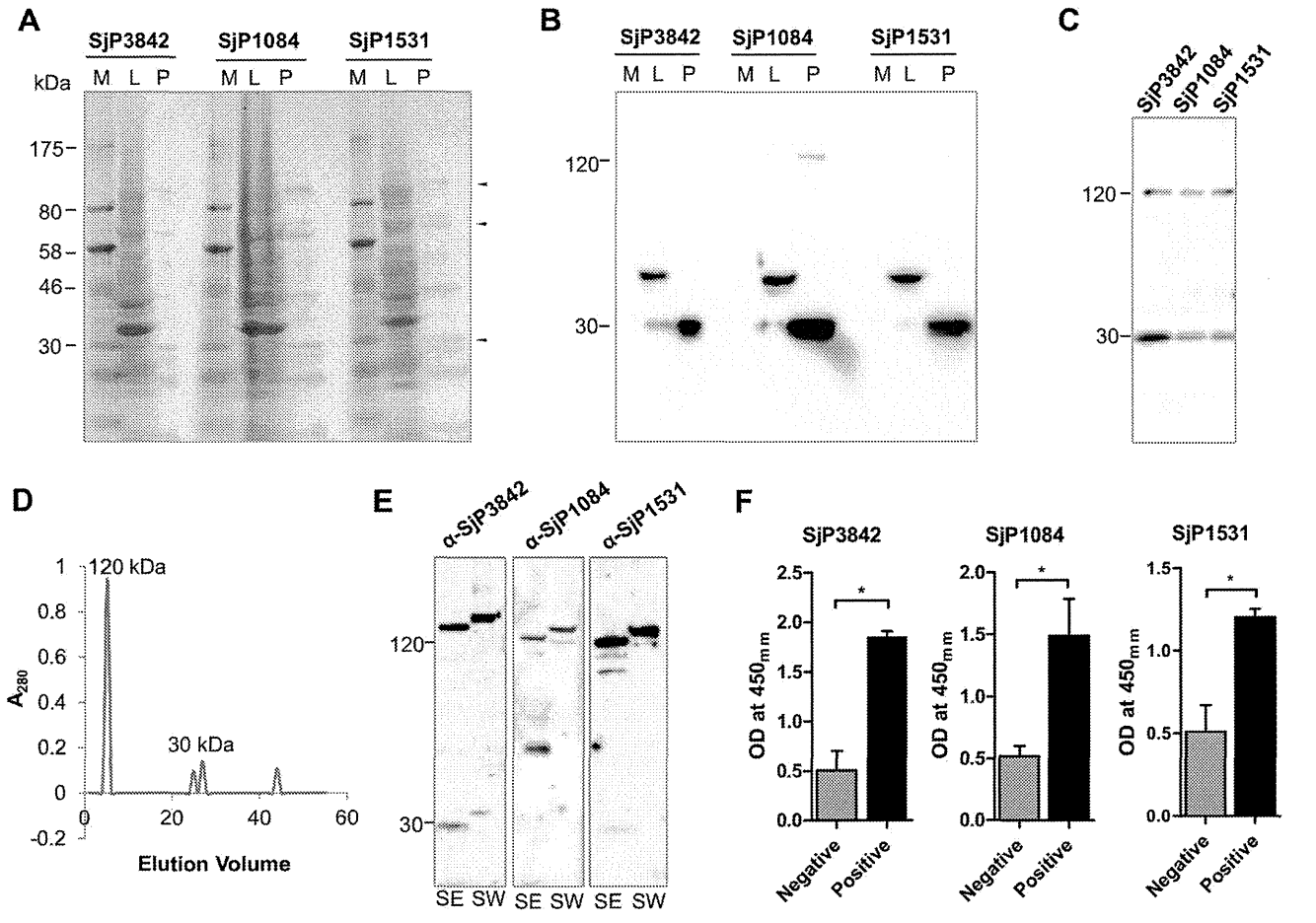

Figure 4. Protein expression and antigenicity of the candidate proteins. (**A**) SDS-PAGE of recombinant *E. coli* lysates (lane L) and purified protein without inclusion bodies (lane P). Arrows indicate expected molecular weights of oligomers. Other bands are expected SEA-domain cleavage products. (**B**) Western blots of recombinant protein expression as in (B), probed with anti-HisG antibody. (**C**) Anti-HisG probed western blots showing oligomerization of proteins with multiple bands of additive ~30 kDa subunits, and tetramer as the most stable state. (**D**) Size exclusion gel filtration chromatography of SjCP3842 showed multiple elution peaks, another evidence of oligomerization. (**E**) Immunoblots showing reactivity of parasite crude antigen preparations (SEA and SWA) with immune sera. (**F**) The candidate proteins specifically reacted with infected miniature pig sera in IgG ELISA, indicating potential antigenicity during schistosomiasis. Bars represent standard deviation (SD). * = $p<0.05$, ** = $p<0.01$. n = 4 for each group.
doi:10.1371/journal.pntd.0002644.g004

using SjCP3842. We first estimated the peroxidase activities of known concentrations of hemin, and used the resulting standard curve (linear graph) to estimate the amount of heme bound by the characterized heme-binding protein based on the peroxidase activity of bound heme (Figure 6D). The result showed that the amount of bound heme increased with increasing protein concentration, reaching saturation at about 2 μg of protein, when 1 μg of hemin was bound (Figure 6D).

To further assess the binding affinity of the protein-heme interaction, optical absorption spectra of the protein-heme complex was monitored by differential titration of 10 μM of heme with increasing concentrations of the protein (0 to 28 μM) (Figure 6E). The Soret absorption peak for heme alone was characteristically broad and was initially 388 nm prior to addition of the protein (broken lines). The Soret absorption maximum was red shifted to 412 nm on addition of protein and absorbance at this peak increased gradually depending on accumulation of protein-heme complex, until saturation at about 1:1 molar ratio. The Q-bands (534 nm and 564 nm) and the isobestic points were also apparent, indicating the presence of two absorbing species (heme and protein-heme complex) in the solution. The UV-visualization spectral attributes of the protein-heme complex (Soret peak, 412 nm; Q-bands, 534 nm and 564 nm) were typical of heme with hexa-coordinated ferric iron [40,43], consistent with the structural model of this study. However, this needs to be confirmed by electron spin resonance spectroscopy. The inset is the heme-binding curve constructed by plotting ΔA_{412} versus protein concentration (Figure 6E). The curve fitting indicates increasing accumulation of the protein-heme complex with saturation after about 10 μM of protein was added, thus suggesting a 1:1 stoichiometry. The fitting yielded equilibrium dissociation constant $K_D = 1.605 \times 10^{-6}$ M, indicating high affinity for binding heme. Taken together, these observations confirm the potential of the novel SEA-domain proteins to specifically interact with heme.

Localization on adult worm teguments and gastrodermis

To ascertain the tissue distribution of the products of this gene family in the parasite, immunolocalization was performed by immunofluorescence assay (IFA) and immunoperoxidase staining. For clarity and because similar tissue localization patterns were observed, only the data for SjCP3842 is shown here. The results for the other candidates are presented in a supplementary figure (Figure S7). IFA on adult worm sections showed that the native

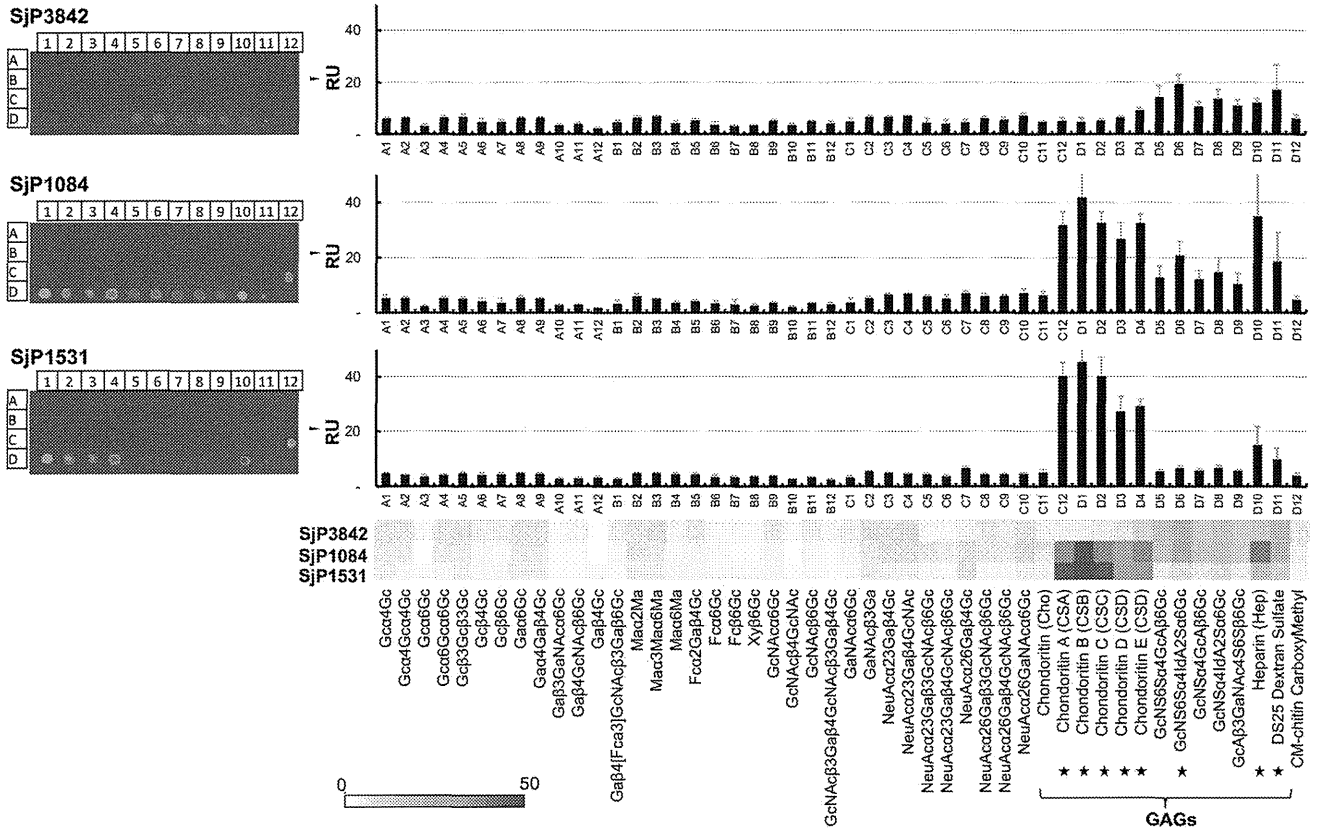

Figure 5. ***S. japonicum*** **SEA-domains mediate binding to glycosaminoglycans (GAGs).** Interactions between glycans and SEA-domain proteins were analyzed using array type sugar chip in SPR system. Shown here are the SPR imaging and SPR signals (RU), which is proportional to the amount of proteins bound to glycans immobilized on sensor chips in an array format. There was high-affinity binding to chondroitin sulfate, heparin, dextran sulfate and other sulfated GAGs. The binding kinetics is shown in Figure S6.
doi:10.1371/journal.pntd.0002644.g005

SjCP3842 was localized on the adult worm tegument and gastrodermis of the parasites gut (Figure 7 A and D). Similar results were observed for all the three candidates as presented in a supplementary figure (Figure S7). No signal was observed in the ovary as shown in the cross section of the female adult worm probed with anti-SjCP3842 monoclonal antibody (Figure 7 B and E), which is consistent with minimal expression in the egg as earlier shown in the developmental stage specific gene expression (Figure 3A). The nuclei are stained with DAPI, showing staining both in the parasite tissues and the content of the ovary. No signal was observed in the sections incubated with sera obtained from control mice (Figure 7 C and F).

Equally, immunolocalization was repeated using immunoperoxidase-DAB technique with biotinylated monoclonal antibody detected with streptavidin-HRP. The result again showed localization on the adult worm teguments (Figure 7 G and H). The protein was also found localized on the tegument of the juvenile schistosomula stage (Figure 7I). No peroxidase activity was detected in the sections probed with pre-immune serum (Figure 7 J–L). Taken together, these results indicate localization on adult worm teguments and gastrodermis, and schistosomula teguments.

Discussion

We have utilized comparative homology modeling to identify remote structural homologs, and successfully characterized a novel gene family encoding SEA-domain proteins from *S. japonicum*. Similar strategy was used to identify and characterize heme-binding property for this domain, thereby providing insight into the potential biological function of otherwise 'hypothetical proteins'. Functional annotation of proteins routinely relies on sequence homology with already characterized proteins or at least domains with experimentally resolved functions. However, the degree of evolutionary conservation of the structural architecture of proteins is greater than the amino acid sequence conservation [24,25]. Our results affirmed that absolute reliance on sequence homology for functional annotation of proteins is not exhaustive. In the post-genome era, the vast accumulation of sequence data has opened new frontiers for identification of intervention targets. However, determination of protein functions is one of the major challenges since sequence homology alone has proven insufficient for placing the vast amount of '*omics*' data into functional context [24,25]. It is necessary to explore other strategies that can effectively identify remote homologs, which are not readily identifiable from sequence data. The data presented here is a typical example of the possible application of molecular structural analysis to identify and characterize novel protein functions.

Like most previously characterized SEA-domain containing proteins, our candidates specifically interacted with sugar chains, especially glycosaminoglycans (GAGs) [28,41]. GAGs are long linear polysaccharides composed of repeating disaccharide units, usually linked covalently to a core protein to form a proteoglycan. While the protein core keeps the proteoglycan localized on the cell surface or in the extracellular matrix (ECM), the GAGs

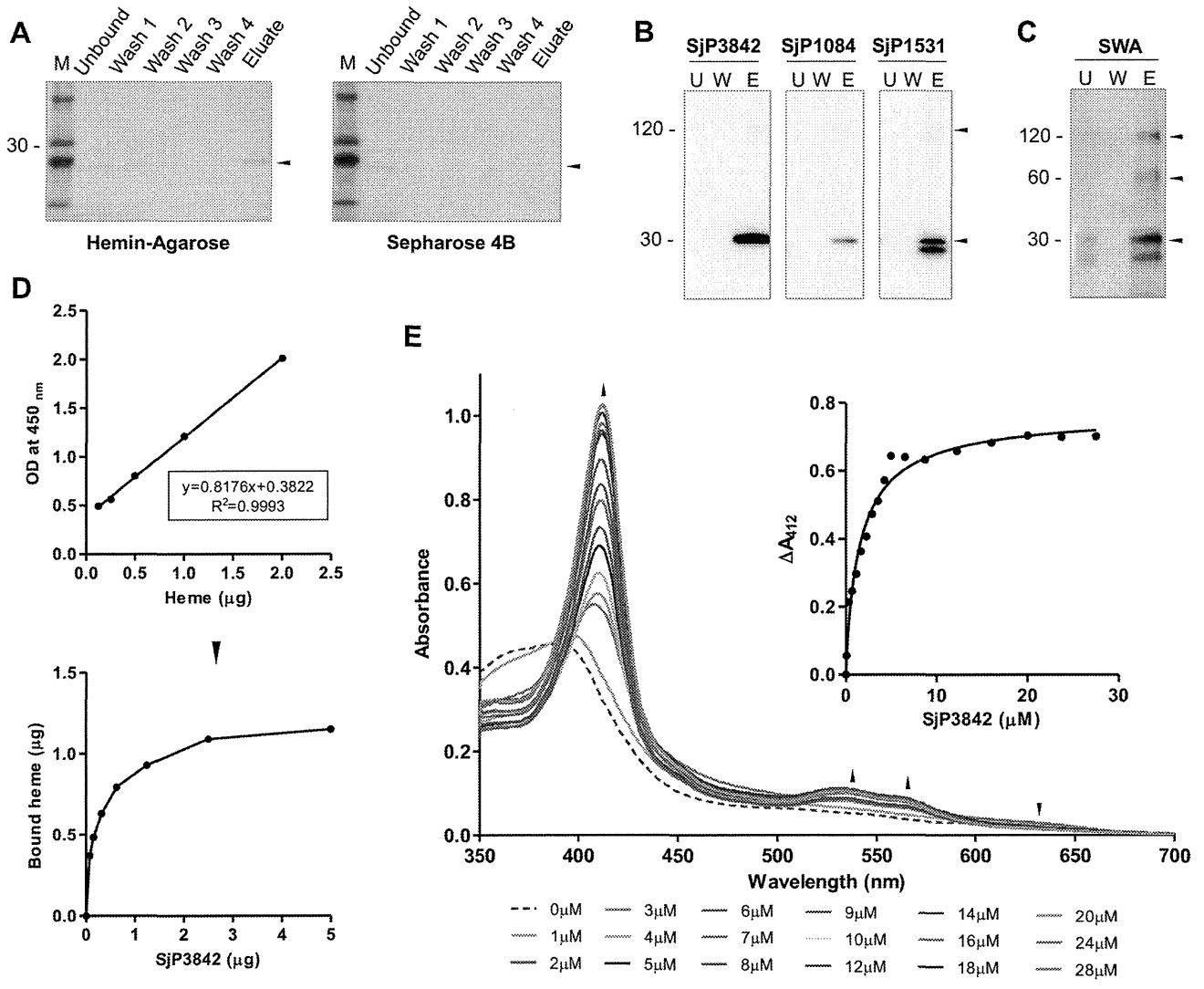

Figure 6. ***S. japonicum*** **SEA-domain proteins are heme-binding proteins.** (**A**) Hemin-agarose binding assay showing potential of SjCP3842 to bind heme on hemin-agarose beads. (**B**) Hemin-agarose binding assay confirmed by immunoblotting using three candidates. 'U': unbound, 'W': last wash, 'E': eluates. (**C**) Identification of SjCP3842 in heme-binding protein fractions from parasite crude extracts (SWA). (**D**) Estimation of the amount of heme bound using peroxidase activity of bound heme. Standard curve (linear graph) of peroxidase activity of known concentrations of hemin was used to estimate the amount of bound heme. (**E**) Differential spectral titration of protein-heme interaction using 10 μM of heme and increasing concentrations of the protein (0 to 28 μM). Soret peak was red shifted from 388 nm to 412 nm, and absorption maximum increased with increasing accumulation of protein-heme complex. The inset is the heme-binding curve constructed by plotting ΔA_{412} versus protein concentration, showing 1:1 stoichiometry.
doi:10.1371/journal.pntd.0002644.g006

components mediate interactions with a plethora of extracellular ligands and effectors. All cellular processes that involve cell surface molecular interactions including: ligand-receptor, cell-cell and cell-matrix interactions, will likely involve proteoglycans and GAGs because these molecules are ubiquitous and are shown to functionally bind proteins to regulate important developmental processes [44–46].

In addition to their space filling and organizational roles in the ECM, GAGs on proteoglycans can modulate the function of a repertoire of extracellular effectors by their roles in: ligand gathering, clustering and oligomerization of ligands and their receptors [45,46], and their ability to act as storage depots for ligands by sequestering them and preventing their rapid degradation [45]. Proteoglycans are required as co-receptors for some growth factors and cytokines signaling in collaboration with the cognate signaling receptors in a ligand-receptor-proteoglycan ternary complex [45–47], and can also signal independently as a receptor via its cytoplasmic domain [47,48]. Proteoglycans can also undergo proteolytic cleavage near the plasma membrane to shed their ectodomain as soluble regulators [49]. Specific interaction with GAGs of host (*trans*) or parasite (*cis*) origin as we observed here may suggest some functional role of this protein family as parasite receptors for accessing ligands and signals, especially of host origin. From the foregoing, and given that *S. japonicum* genome encodes many receptors and signaling molecules but sometimes not the ligands [21], it is plausible that parasite membrane receptors with GAG-binding potential could interact with its own or host proteoglycans in a receptor-proteoglycan-ligand ternary complex [45–47], as a means of accessing host molecules tethered on GAGs for signals for their growth,

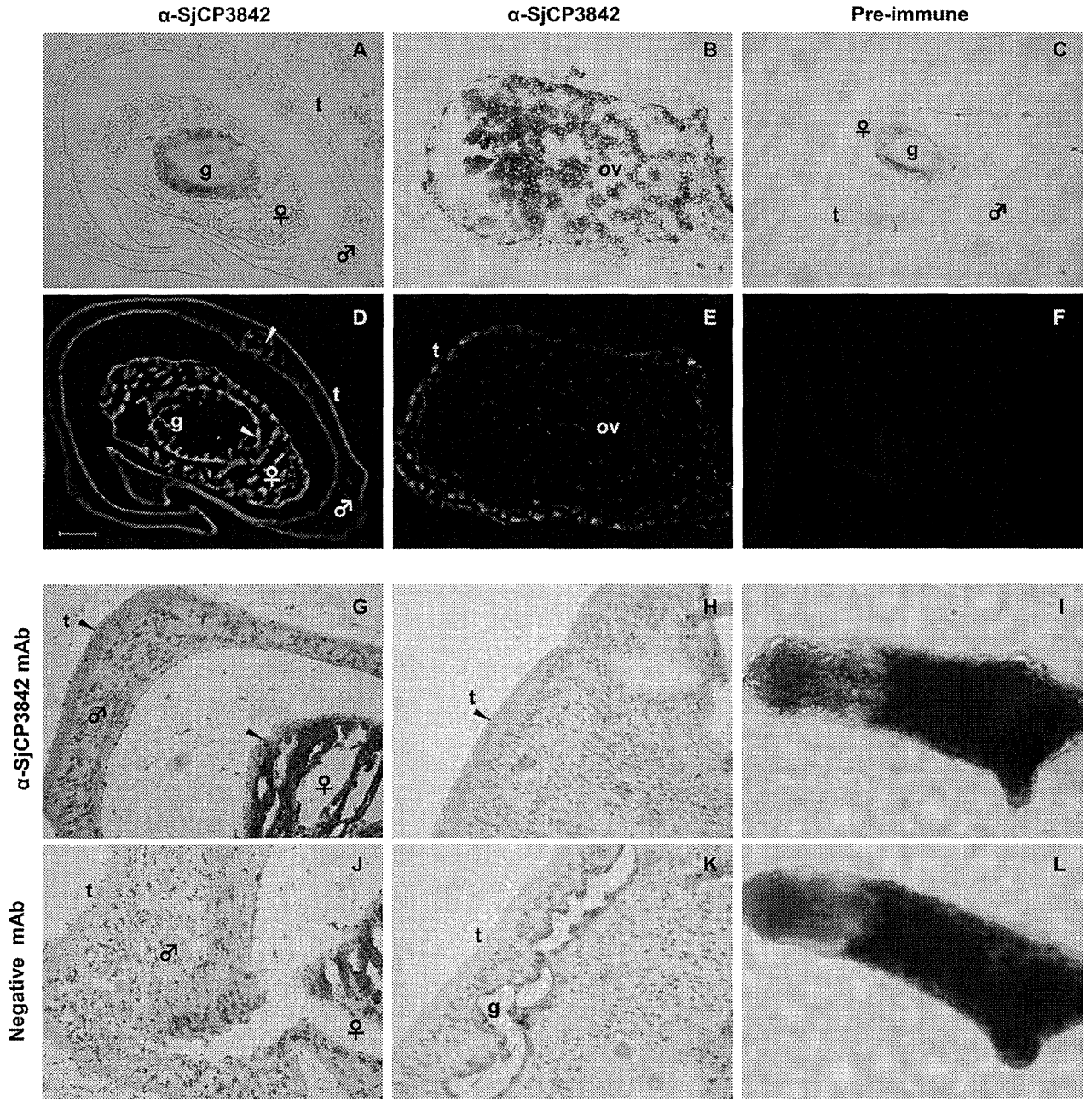

Figure 7. Immunolocalization on the teguments and gastrodermis. Tissue localization of native SjCP3842 was shown using immunofluorescence (A–F) and immunoperoxidase (G–L) methods. (**A**) Bright field image of cross section of adult worm pair. (**B**) Bright field image of cross section of female adult worm showing the ovary. (C) Bright field image of a cross section of adult worm pair for control IFA. (**D**) IFA on a cross section of adult worm pair using monoclonal antibody showed that the native SjCP3842 was localized on the adult worm tegument (t) and gastrodermis (yellow arrows) of the parasites gut (g). Scale bar = 50 μm. (**E**) IFA on a cross section of a female worm showing FITC staining of SjCP3842 on adult worm teguments but not in the content of the ovary. DAPI staining of nuclei was detected in the tissue and ovary. (**F**) IFA using pre-immune serum as negative control. (**G** and **H**) Immunoperoxidase detection (brown) of SjCP3842 in a section of adult worm pair showed localization on adult worm tegument. (**I**) Immunoperoxidase localization of SjCP3842 on juvenile schistosomula showed localization on the tegument. Negative immunoperoxidase detection was observed in sections of adult worm (**J** and **K**) and schistosomulae (**L**) probed with pre-immune serum.
doi:10.1371/journal.pntd.0002644.g007

development, and maturation thus rendering them potential intervention targets.

The native proteins were localized at the parasite tegument and gastrodermis, sites that are of immunological significance being located at the host-parasite interface [14,16]. These sites are rich in proteins that are often unique to schistosomes, some of which can directly interact with host derived molecules as observed in the characterized SEA-domain proteins [14,16]. The ability of the parasite to bind GAGs on host secreted or shed proteoglycans [49] or proteoglycans on the surface of host immune cells [50] could result in masking of the 'non-self' status of the parasite, thereby evading attack by host immune system [51]. It is thus possible from the foregoing, that this gene family could also be involved in some immune evasion mechanisms. We are presently targeting the

candidates that are expressed at the infective cercarial, schistosomula and adult stages for possible vaccine application.

Heme-binding properties have been described here for the first time for SEA-domain proteins from this hemophagous parasite. In terms of the parasite biology and host-parasite interaction, this finding represents a significant contribution towards elucidating heme detoxification and heme iron acquisition mechanisms of the parasite. Schistosomes inhabit the hepatoportal veins of the host, where they feed on host erythrocytes and catabolize the globin moieties of hemoglobin as a major source of the requisite amino acids for their growth, development and reproduction [3,4]. However, the released heme moiety is potentially toxic due to its reactive nature and ability to produce free radical species, lipid peroxidation, and protein and DNA oxidation [3,6]. Hemophagy-adapted parasites have therefore evolved strategies to sequester and detoxify heme [3–9]. Heme iron is arguably the major source of iron for this parasite, thus, the parasite also maintains a heme acquisition mechanism to harness the needed iron from heme molecules [4,10]. These candidates are localized on adult worm gastrodermis, the site for heme detoxification [8,17] and acquisition [3,10]; and in the adult and schistosomula teguments, also potential sites for heme acquisition in these stages [20]. Indeed, effective heme homeostasis mechanism is paramount for parasite survival and establishment, and is a major target of effective drugs against hemoparasites including the *quinines* and *artemisinine* [11–13]. Unfortunately, the exact mechanisms and the molecules involved in heme-homeostasis are still controversial. However, there is a consensus on the involvement of heme-binding proteins both as nucleation agents for heme crystallization [6–8,17], and as surface heme receptors in an ABC- (ATP binding cassette) transporters coupled heme uptake mechanism [38,52,53].

The developmental stage specific expression, especially of SjCP3842, clearly showed overt expression at the adult stage especially the female adult worms, which is consistent with the heme homeostasis requirements of this stage. There was also relatively high expression in the snail inhabiting sporocysts and the infective cercariae. The observation that the sporocysts also express this gene indicates expression at the snail stage as well, which may suggest similar or different function in the snail host. With regards to heme binding function, the sporocysts are known to absorb nutrients from snail host through their tegument for nourishment of cercariae in their germinal sac [54], and heme binding proteins have also been identified among secreted proteins from the sporocyst stage [55]. Since iron source in snail is mainly in the form of heme, it is plausible that heme binding proteins like the ones we characterized might be required for heme iron uptake from snail hosts, as well as other functions. SEA domain still do not have a well characterized function apart from interaction with glycans (GAGs), to which we and others have alluded several potential implications like ligand acquisition and immune evasion. The prospect that this gene family could perform more than one function in different developmental stages of the parasite implies that hemophagy might have been a major factor among other selection factors for this gene family.

SEA-domains are characteristically found in carbohydrate rich mucous environments [30]. The heme-binding SEA-domain proteins we described here are localized in the parasite gastrodermis and tegument. The gastrodermis is the syncytial linings of the parasite gut, the site for hemoglobin catabolism, heme sequestration, detoxification and acquisition. A similar structure called peritrophic matrix (PM) with heme-binding property has been described in the midgut of hemophagous insects. The PMs perform a central role in heme homeostasis by protecting the insects' midgut against damage from heme toxicity [56], akin to schistosomes gastrodermis. The PMs are complex matrices composed of heme-binding proteins, proteoglycans, chitins and chitin-binding proteins [56]. Specifically, *Aedes aegypti* Mucin I (*Ae*MUC1) was identified as a major heme-binding protein in the PM [57]. MUC1 and the proteins we characterized here both contain SEA-domains. It is therefore plausible that similar mechanism mediated by heme-binding SEA-domain proteins may exist in schistosomes' gastrodermis. However, this hypothesis will need to be experimentally clarified by isolating and identifying all heme-binding proteins of the parasite and/or the parasite gastrodermis. We will design further studies to fully characterize the role of this gene family in the parasite heme-homeostasis and heme acquisition mechanisms, and explore prospects for its application in disease intervention.

Supporting Information

Figure S1 Multiple alignments and molecular structures of the SEA-domain proteins from *S. japonicum*. (**A**) Multiple alignments of SST isolated candidates showing similar signal sequence [27]. (**B**) The Topology of the members of the gene family. (**C**) The modeled molecular structures of whole molecules showing the SEA-domain. (**D**) Predicted oligomeric state of SjCP3842 as a representative of the family.
(TIF)

Figure S2 Glycoprotein detection analysis showed evidence of *O*-linked glycosylation in the expressed candidate proteins. We showed using glycosylation detection assay that the expressed proteins contain *O*-linked glycans. Glycosylated proteins were detected as magenta stained bands in SDS-PAGE fractions.
(TIF)

Figure S3 Molecular structure based identification of heme-binding site. 3DLigandSite ligand binding site prediction report showing structure based identification of heme-binding site at highly significant precision. The heme-binding site was predicted based on 178 ligands present in 177 homologous structures.
(PDF)

Figure S4 Heme-binding pocket of SjCP3842. (**A**) Heme-binding mode of SjCP3842 showing the hydrophobic vinyl end of heme inserted into a hydrophobic cavity, while hydrophilic propionate end points away from the pocket. Heme is represented using spheres model colored by atoms (C: green, N: blue, O: red, Fe: brown). (**B**) The interacting residues in the heme-binding site. Strictly conserved residues are labeled in red while partly conserved residues are labeled in blue. Heme molecule is shown with nb-spheres model while residues are shown with sticks model, both colored by atoms. (**C**) The second predicted heme-binding mode showing heme iron hexa-coordinated with His-149 and Met-50 as axial ligands.
(TIF)

Figure S5 Heme binding pocket of SjCP1531. Similar binding site characteristics as observed for SjCP3842 were observed for SjCP1531. However, heme iron is coordinated to Tyr-154 as its axial ligand. (**A**) Heme-binding mode of SjCP1531 showing the hydrophobic vinyl end of the protoporphyrin heme inserted into a hydrophobic cavity, while hydrophilic propionate ends of points away from the pocket. Heme is represented using spheres model colored by atoms (C: green, N: blue, O: red, Fe: brown). The protein is shown using cartoon model. (**B**) Heme-binding site showing the Connolly surface of the binding pocket

(dots). (**C**) Heme iron (brown sphere) putatively coordinated to Tyr-154 as axial ligand.
(TIF)

Figure S6 Specificity and affinity of protein-glycan interactions. (**A**) Array format of CS-GAG chip. (**B**) SPR imaging of the glycan-binding assay are shown. (**C**) Sensorgram and binding curve of the interaction between SjCP1084 and chondroitin sulfate-E as representative of the binding kinetics data. (**D**) Summary of equilibrium dissociation constants (K_D) of protein-glycan interactions, showing values within nanomolar range.
(TIF)

Figure S7 Immunolocalization on the teguments and gut epithelial linings. Immunolocalization of SjCP1084 (**A** and **D**) and SjCP1531 (**B** and **E**) using IFA on cross sections of adult worm pairs probed with immune sera and detected with FITC conjugated secondary antibody. Immunoperoxidase detection of SjCP1084 (**G**) and SjCP1531 (**H**) on the juvenile schistosomulae using immune sera and HRP conjugated secondary antibodies also showed localization on the tegument. No signal was detected in adult worm sections and schistosomulae probed with the pre-immune serum (**C, F** and **I**).
(TIF)

Table S1 Summary of structural homology modeling results for *S. japonicum* SEA-domain gene family. In addition to the structural homology modeling data presented in Figure 1, the structural modeling was equally performed for all identified transcripts in this gene family and the result is summarized in this table.
(DOCX)

Table S2 Developmental stage specific expression of *Schistosoma japonicum* SEA-domain containing genes. The developmental stage specific expression of the candidate genes expressed as copy number per nanogram of cDNA. The detailed data statistics of the data plotted in Figure 3 is reproduced here to show mean values and standard deviations of each candidate at each developmental stage of the parasite.
(DOCX)

Acknowledgments

We are grateful to Drs. Masachika Senba and Tetsuo Yanagi of NEKKEN Nagasaki University, and Dr. Takashi Kumagai of TMDU Tokyo for technical support. We thank the members of Prof. Hirayama's Laboratory (Department of Immunogenetics, NEKKEN, Nagasaki University) for useful suggestions and insightful discussion.

Author Contributions

Conceived and designed the experiments: ECM MK KH. Performed the experiments: ECM MK NTH MNS CY MSC MW YS. Analyzed the data: ECM MK NTH MNS YS KH. Contributed reagents/materials/analysis tools: MK CY MW YS KH. Wrote the paper: ECM KH.

References

1. Chitsulo L, Engels D, Montresor A, Savioli L (2000) The global status of schistosomiasis and its control. Acta Trop 77: 41–51.
2. Tran MH, Pearson MS, Bethony JM, Smyth DJ, Jones MK, et al. (2006) Tetraspanins on the surface of Schistosoma mansoni are protective antigens against schistosomiasis. Nat Med 12: 835–840.
3. Toh SQ, Glanfield A, Gobert GN, Jones MK (2010) Heme and blood-feeding parasites: friends or foes? Parasit Vectors 3: 108.
4. Glanfield A, McManus DP, Anderson GJ, Jones MK (2007) Pumping iron: a potential target for novel therapeutics against schistosomes. Trends Parasitol 23: 583–588.
5. Paiva-Silva GO, Cruz-Oliveira C, Nakayasu ES, Maya-Monteiro CM, Dunkov BC, et al. (2006) A heme-degradation pathway in a blood-sucking insect. Proc Natl Acad Sci U S A 103: 8030–8035.
6. Graça-Souza AV, Maya-Monteiro C, Paiva-Silva GO, Braz GR, Paes MC, et al. (2006) Adaptations against heme toxicity in blood-feeding arthropods. Insect Biochem Mol Biol 36: 322–335.
7. Chugh M, Sundararaman V, Kumar S, Reddy VS, Siddiqui WA, et al. (2013) Protein complex directs hemoglobin-to-hemozoin formation in Plasmodium falciparum. Proc Natl Acad Sci U S A 110: 5392–5397.
8. Oliveira MF, d'Avila JC, Torres CR, Oliveira PL, Tempone AJ, et al. (2000) Haemozoin in Schistosoma mansoni. Mol Biochem Parasitol 111: 217–221.
9. Egan TJ (2008) Haemozoin formation. Mol Biochem Parasitol 157: 127–136.
10. Rao AU, Carta LK, Lesuisse E, Hamza I (2005) Lack of heme synthesis in a free-living eukaryote. Proc Natl Acad Sci U S A 102: 4270–4275.
11. Corrêa Soares JB, Menezes D, Vannier-Santos MA, Ferreira-Pereira A, Almeida GT, et al. (2009) Interference with hemozoin formation represents an important mechanism of schistosomicidal action of antimalarial quinoline methanols. PLoS Negl Trop Dis 3: e477.
12. Oliveira MF, d'Avila JC, Tempone AJ, Soares JB, Rumjanek FD, et al. (2004) Inhibition of heme aggregation by chloroquine reduces Schistosoma mansoni infection. J Infect Dis 190: 843–852.
13. Kumar S, Guha M, Choubey V, Maity P, Bandyopadhyay U (2007) Antimalarial drugs inhibiting hemozoin (beta-hematin) formation: a mechanistic update. Life Sci 80: 813–828.
14. Van Hellemond JJ, Retra K, Brouwers JF, van Balkom BW, Yazdanbakhsh M, et al. (2006) Functions of the tegument of schistosomes: clues from the proteome and lipidome. Int J Parasitol 36: 691–699.
15. Delcroix M, Medzihradsky K, Caffrey CR, Fetter RD, McKerrow JH (2007) Proteomic analysis of adult S. mansoni gut contents. Mol Biochem Parasitol 154: 95–97.
16. Mulvenna J, Moertel L, Jones MK, Nawaratna S, Lovas EM, et al. (2010) Exposed proteins of the Schistosoma japonicum tegument. Int J Parasitol 40: 543–554.
17. Corrêa Soares JB, Maya-Monteiro CM, Bittencourt-Cunha PR, Atella GC, Lara FA, et al. (2007) Extracellular lipid droplets promote hemozoin crystallization in the gut of the blood fluke Schistosoma mansoni. FEBS Lett 581: 1742–1750.
18. Chen MM, Shi L, Sullivan DJ (2001) Haemoproteus and Schistosoma synthesize heme polymers similar to Plasmodium hemozoin and beta-hematin. Mol Biochem Parasitol 113: 1–8.
19. Stiebler R, Soares JB, Timm BL, Silva JR, Mury FB, et al. (2011) On the mechanisms involved in biological heme crystallization. J Bioenerg Biomembr 43: 93–99.
20. Clemens LE, Basch PF (1989) Schistosoma mansoni: effect of transferrin and growth factors on development of schistosomula in vitro. J Parasitol 75: 417–421.
21. Consortium SjGSaFA (2009) The Schistosoma japonicum genome reveals features of host-parasite interplay. Nature 460: 345–351.
22. Hu W, Yan Q, Shen DK, Liu F, Zhu ZD, et al. (2003) Evolutionary and biomedical implications of a Schistosoma japonicum complementary DNA resource. Nat Genet 35: 139–147.
23. Liu F, Cui SJ, Hu W, Feng Z, Wang ZQ, et al. (2009) Excretory/secretory proteome of the adult developmental stage of human blood fluke, Schistosoma japonicum. Mol Cell Proteomics 8: 1236–1251.
24. Ebihara A, Okamoto A, Kousumi Y, Yamamoto H, Masui R, et al. (2005) Structure-based functional identification of a novel heme-binding protein from Thermus thermophilus HB8. J Struct Funct Genomics 6: 21–32.
25. Sivashankari S, Shanmughavel P (2006) Functional annotation of hypothetical proteins - A review. Bioinformation 1: 335–338.
26. Yu C, Zhang F, Yin X, Kikuchi M, Hirayama K (2008) Isolation of the cDNAs encoding secreted and membrane binding proteins from egg of Schistosoma japonicum (Chinese strain). Acta Parasitologica 1: 110–114.
27. Mbanefo EC, Yu C, Kikuchi M, Shuaibu NM, Boamah D, et al. (2012) Origin of a novel protein-coding gene family with similar signal sequence in Schistosoma japonicum. BMC Genomics 13: 260.
28. Bork P, Patthy L (1995) The SEA module: a new extracellular domain associated with O-glycosylation. Protein Sci 4: 1421–1425.
29. Maeda T, Inoue M, Koshiba S, Yabuki T, Aoki M, et al. (2004) Solution structure of the SEA domain from the murine homologue of ovarian cancer antigen CA125 (MUC16). J Biol Chem 279: 13174–13182.
30. Palmai-Pallag T, Khodabukus N, Kinarsky L, Leir SH, Sherman S, et al. (2005) The role of the SEA (sea urchin sperm protein, enterokinase and agrin) module in cleavage of membrane-tethered mucins. FEBS J 272: 2901–2911.
31. Corpet F (1988) Multiple sequence alignment with hierarchical clustering. Nucleic Acids Res 16: 10881–10890.
32. Gupta R, Brunak S (2002) Prediction of glycosylation across the human proteome and the correlation to protein function. Pac Symp Biocomput: 310–322.
33. Kelley LA, Sternberg MJ (2009) Protein structure prediction on the Web: a case study using the Phyre server. Nat Protoc 4: 363–371.
34. Raman S, Vernon R, Thompson J, Tyka M, Sadreyev R, et al. (2009) Structure prediction for CASP8 with all-atom refinement using Rosetta. Proteins 77 Suppl 9: 89–99.

35. Wass MN, Kelley LA, Sternberg MJ (2010) 3DLigandSite: predicting ligand-binding sites using similar structures. Nucleic Acids Res 38: W469–473.
36. Tansatit T, Sahaphong S, Riengrojpitak S, Viyanant V, Sobhon P (2006) Immunolocalization of cytoskeletal components in the tegument of the 3-week-old juvenile and adult Fasciola gigantica. Vet Parasitol 135: 269–278.
37. Suda Y, Arano A, Fukui Y, Koshida S, Wakao M, et al. (2006) Immobilization and clustering of structurally defined oligosaccharides for sugar chips: an improved method for surface plasmon resonance analysis of protein-carbohydrate interactions. Bioconjug Chem 17: 1125–1135.
38. Asuthkar S, Velineni S, Stadlmann J, Altmann F, Sritharan M (2007) Expression and characterization of an iron-regulated hemin-binding protein, HbpA, from Leptospira interrogans serovar Lai. Infect Immun 75: 4582–4591.
39. Huy NT, Xuan Trang DT, Uyen DT, Sasai M, Harada S, et al. (2005) An improved colorimetric method for quantitation of heme using tetramethylbenzidine as substrate. Anal Biochem 344: 289–291.
40. Huy NT, Kamei K, Yamamoto T, Kondo Y, Kanaori K, et al. (2002) Clotrimazole binds to heme and enhances heme-dependent hemolysis: proposed antimalarial mechanism of clotrimazole. J Biol Chem 277: 4152–4158.
41. Akhavan A, Crivelli SN, Singh M, Lingappa VR, Muschler JL (2008) SEA domain proteolysis determines the functional composition of dystroglycan. FASEB J 22: 612–621.
42. Levitin F, Stern O, Weiss M, Gil-Henn C, Ziv R, et al. (2005) The MUC1 SEA module is a self-cleaving domain. J Biol Chem 280: 33374–33386.
43. Huy NT, Serada S, Trang DT, Takano R, Kondo Y, et al. (2003) Neutralization of toxic heme by Plasmodium falciparum histidine-rich protein 2. J Biochem 133: 693–698.
44. Lin X (2004) Functions of heparan sulfate proteoglycans in cell signaling during development. Development 131: 6009–6021.
45. Tumova S, Woods A, Couchman JR (2000) Heparan sulfate proteoglycans on the cell surface: versatile coordinators of cellular functions. Int J Biochem Cell Biol 32: 269–288.
46. Derksen PW, Keehnen RM, Evers LM, van Oers MH, Spaargaren M, et al. (2002) Cell surface proteoglycan syndecan-1 mediates hepatocyte growth factor binding and promotes Met signaling in multiple myeloma. Blood 99: 1405–1410.
47. Chua CC, Rahimi N, Forsten-Williams K, Nugent MA (2004) Heparan sulfate proteoglycans function as receptors for fibroblast growth factor-2 activation of extracellular signal-regulated kinases 1 and 2. Circ Res 94: 316–323.
48. Couchman JR (2010) Transmembrane signaling proteoglycans. Annu Rev Cell Dev Biol 26: 89–114.
49. Nam EJ, Park PW (2012) Shedding of cell membrane-bound proteoglycans. Methods Mol Biol 836: 291–305.
50. Wegrowski Y, Milard AL, Kotlarz G, Toulmonde E, Maquart FX, et al. (2006) Cell surface proteoglycan expression during maturation of human monocytes-derived dendritic cells and macrophages. Clin Exp Immunol 144: 485–493.
51. van Die I, Cummings RD (2010) Glycan gimmickry by parasitic helminths: a strategy for modulating the host immune response? Glycobiology 20: 2–12.
52. Sook BR, Block DR, Sumithran S, Montañez GE, Rodgers KR, et al. (2008) Characterization of SiaA, a streptococcal heme-binding protein associated with a heme ABC transport system. Biochemistry 47: 2678–2688.
53. Cupello MP, Souza CF, Buchensky C, Soares JB, Laranja GA, et al. (2011) The heme uptake process in Trypanosoma cruzi epimastigotes is inhibited by heme analogues and by inhibitors of ABC transporters. Acta Trop 120: 211–218.
54. Walker AJ (2011) Insights into the functional biology of schistosomes. Parasit Vectors 4: 203.
55. Wu XJ, Sabat G, Brown JF, Zhang M, Taft A, et al. (2009) Proteomic analysis of Schistosoma mansoni proteins released during in vitro miracidium-to-sporocyst transformation. Mol Biochem Parasitol 164: 32–44.
56. Pascoa V, Oliveira PL, Dansa-Petretski M, Silva JR, Alvarenga PH, et al. (2002) Aedes aegypti peritrophic matrix and its interaction with heme during blood digestion. Insect Biochem Mol Biol 32: 517–523.
57. Devenport M, Alvarenga PH, Shao L, Fujioka H, Bianconi ML, et al. (2006) Identification of the Aedes aegypti peritrophic matrix protein AeIMUCI as a heme-binding protein. Biochemistry 45: 9540–9549.

Efficacy and Safety of Switching from Basal Insulin to Sitagliptin in Japanese Type 2 Diabetes Patients

Authors
S.-I. Harashima[1], D. Tanaka[1], S. Yamane[1], M. Ogura[1], Y. Fujita[1], Y. Murata[2], M. Seike[2], T. Koizumi[2], M. Aono[2], Y. Wang[1], N. Inagaki[1]

Affiliations
[1] Department of Diabetes and Clinical Nutrition, Graduate School of Medicine, Kyoto University, Kyoto, Japan
[2] Department of Internal Medicine, Takashima General Hospital, Takashima, Japan

Key words
- sitagliptin
- basal insulin
- insulin secretion capacity

Abstract

Basal-supported oral therapy (BOT) is often used to treat poorly controlled type 2 diabetes. However, patients sometimes experience nocturnal and early morning hypoglycemia. Thus, maintaining targeted glycemic control by BOT is limited in some patients. We assessed the efficacy and safety of replacing basal insulin by sitagliptin therapy in Japanese type 2 diabetes patients on BOT. Forty-nine subjects were sequentially recruited for the 52-week, prospective, single arm study. Patients on BOT therapy were switched from basal insulin to sitagliptin. The primary endpoint was change in HbA1c in 52 weeks. The secondary endpoints were dropout rate, changes in body weight, frequency of hypoglycemia, and relationship between change in HbA1c and insulin secretion capacity evaluated by glucagon loading test. The average dose of basal insulin was 15.0±8.4 units. Sixteen subjects (31.3%) were dropped because replacement by sitagliptin was less effective for glycemic control. In these subjects, diabetes duration was longer, FPG and HbA1c at baseline were higher, and insulin secretion capacity was lower. Change in HbA1c in 52 weeks was −4 mmol/mol (95% CI −5 to −4 mmol/mol) ($p<0.05$). Change in body weight was −0.71 kg (95% CI −1.42 to −0.004 kg) ($p<0.05$). Frequency of hypoglycemia was decreased from 1.21±1.05 to 0.06±0.24 times/month. HbA1c level was improved if C-peptide index (CPI) was over 1.19. In conclusion, basal insulin in BOT can be replaced by sitagliptin with a decrease in HbA1c level and frequency of hypoglycemia in cases where insulin secretion capacity was sufficiently preserved.

received 29.05.2012
accepted 13.08.2012

Bibliography
DOI http://dx.doi.org/10.1055/s-0032-1323763
Published online: September 12, 2012
Horm Metab Res 2013; 45: 231–238

ISSN 0018-5043

Correspondence
S.-I. Harashima MD, PhD
Department of Diabetes and Clinical Nutrition
Graduate School of Medicine
Kyoto University
Kyoto 606-8507
Japan
Tel.: +81/75/751 3560
Fax: +81/75/771 6601
harasima@metab.kuhp.kyoto-u.ac.jp

Introduction

Basal insulin preparation is recommended by the American Diabetes Association (ADA)/European Association for the Study of Diabetes (EASD) consensus algorithm when lifestyle interventions and oral glucose-lowering agents no longer achieve the glycemic goal of hemoglobin A1c (HbA1c) level less than 53 mmol/mol [1,2]. Recently, 2 long-acting insulin analogues, insulin glargine and insulin detemir, are available that attain glycemic targets more effectively and safely [3,4]. There are no significant differences reported in glycemic control and overall hypoglycemia between the 2 analogues [5]. The combination of basal insulin and oral hypoglycemic agents (OHAs), known as basal-supported oral therapy (BOT), is often used to treat poorly controlled type 2 diabetes [6,7]. Better glycemic control, fewer hypoglycemic episodes, and less weight gain are obtained by BOT than by biphasic insulin [8]. In addition, BOT is relatively cost effective with the same glycemic control level as biphasic insulin regimen [9]. BOT is also helpful in Japanese type 2 diabetes patients. In the ALOHA (Add-on to Lantus® to OHA) study, in which 5223 Japanese type 2 diabetes patents participated, mean HbA1c was reduced from 75±13 to 60±13 mmol/mol in 24 weeks [10]. Although BOT is well-tolerated and effective for glycemic control, patients sometimes experience nocturnal and early morning hypoglycemia. In the ALOHA study, 0.97% of the patients experienced frequent hypoglycemia. In the 4 T-study, 1.3% of BOT-treated patients experienced hypoglycemia with loss of consciousness [8]. Another problem of BOT is that postprandial glucose is high, although morning fasting blood glucose level is within normal range. An increase in dosage of basal insulin or sulfonyl ureas (SUs); which are most commonly administrated in BOT-treated Japanese patients, is not always effective, and can result in increased hypoglycemia. In Japanese interview forms, frequency of hypoglyc-

emia induced by SUs is reported to be 1.3–2.8%. Thus, maintaining targeted glycemic control by BOT is limited in some patients.

Dipeptidyl peptidase-4 (DDP-4) inhibitor is a newly developed OHA that prevents degradation of the incretin hormones, glucagon-like peptide-1, and gastric inhibitory polypeptide [11]. This compound stimulates glucose-dependent insulin secretion and suppresses glucagon release, and can improve both fasting and postprandial glucose levels. Four different DPP-4 inhibitors are available in Japan: sitagliptin, vildagliptin, alogliptin, and linagliptin. Of these, sitagliptin is most widely used, partly because it was the first approved DPP-4 inhibitor and the safety and efficacy are acceptable in Japanese clinical practice. Generally, sitagliptin is more effective for glycemic control in Japanese patients compared to Caucasian patients [12,13]. Sitaglipitn is usually combined with low dosage of SUs in Japan, less than or equal to 2 mg/day of glimepiride and 40 mg/day of gliclazide, which is enough for glycemic control when combined with sitagliptin [14]. Patients also show improved glycemic control even if insulin secretion capacity is insufficient for oral therapy [14,15]. The main pathophysiology of Japanese type 2 diabetes is impairment of insulin secretion [16,17]. Insulin secretion capacity in Japanese populations is only about half of that in Caucasians [18]. Both decreased basal and early phase insulin secretion contribute more to Japanese type 2 diabetes [16], and insulin therapy is usually required in those with C-peptide index (CPI) lower than 0.8 [19]. However, basal insulin therapy is not always ideal in some patients because postprandial glucose is still high and preprandial glucose is low, which results in large fluctuations in blood glucose. On the other hand, DPP-4 inhibitor might nevertheless ameliorate decreased early phase insulin secretion. This encouraged us to consider whether basal insulin can be replaced with sitagliptin in type 2 diabetes patients treated with SUs and basal insulin in at least some BOT cases.

We show here that sitagliptin can be switched from basal insulin in patients with C-peptide index (CPI) and/or secretory unit of islet in transplantation (SUIT) equal to or larger than 1.19 and/or 36.4, respectively, with beneficial effects on glycemic control.

Materials and Methods

Study design and participants

This was a prospective, 52-week, single center, and single arm intervention study to evaluate the effects on glycemic control of replacement of basal insulin to sitagliptin in type 2 diabetes patients inadequately controlled with BOT. Outpatients of Takashima General Hospital were recruited consecutively for a sample size of 45 subjects. Inclusion criteria were: type 2 diabetes treated with basal insulin (insulin glargine or detemir) and SUs (glimepiride or gliclazide) ± metformin ± thiazolidinedione ± α-glucosidase inhibitors for more than 1 year; aged ≥ 20 years; HbA1c level ≥ 52 mmol/mol; no improvement in HbA1c ≥ 5 mmol/mol within 3 months in BOT; and a fasting C-peptide reactin (CPR) of > 0.5 ng/ml. Exclusion criteria were: type 1 diabetes; secondary diabetes; alcoholism; severe depression, or severe psychological condition; malignancy; and abnormal hemoglobinemia. The study protocol was approved by the Institutional Review Board of Takashima General Hospital, and registered at the University hospital Medical Information Network in Japan (UMIN000005499). Written informed consent was obtained from all subjects.

Procedures and intervention

The duration of the study was 52 weeks. Subjects were screened for eligibility and gave basic demographic information, medical history, and frequency of hypoglycemia. Within a month before changing therapy from basal insulin to sitagliptin, glucagon loading test was performed without any OHAs or basal insulin for more than 24 h to evaluate insulin secretion capacity. When basal insulin was replaced by sitagliptin, the dosage of glimepiride or gliclazide was decreased to equal to or less than 2.0 mg/day or 40 mg/day, respectively, to prevent increased hypoglycemia if the subjects had been treated with more than 2.0 mg/day glimepiride or 40 mg/day gliclazide. If the subjects had been treated with equal to or less than 2.0 mg/day of glimepride or 40 mg/day of gliclazide, that dosage of SUs was maintained. Metformin (Met) and thiazolidinedione (TZD) were continued without any changes during the study. α-Glucosidase inhibitors were discontinued. The dosage of SUs was changed depending on the frequency of hypoglycemic episodes and glycemic control level. Sitagliptin was started at 50 mg/day, the usual initial dosage in Japan, which was increased to 100 mg/day if the HbA1c level did not reach 52 mmol/mol, since titration to 100 mg/day is acceptable.

Measurements

The primary endpoint was the change in HbA1c in 52 weeks. The secondary endpoints were dropout rate due to lesser efficacy of replacement by sitagliptin of basal insulin on glycemic control, change in body weight in 52 weeks, change in body mass index (BMI) in 52 weeks, change in frequency of hypoglycemia in 52 weeks, adverse events, and the correlation between change in HbA1c at the 8th week and insulin secretion capacity or CPI or SUIT at baseline. HbA1c are expressed in mmol/mol according to the recommendation of IFCC. CPI was calculated by the formula: [100 × fasting CPR (ng/ml)]/[18 × FPG (mM)] [19]. SUIT index was calculated by the formula: [250 × fasting CPR (nM)]/[(FPG − 3.43) (mM)] [20]. Blood glucose and C-peptide level were measured before (0 min) and 6 min after intravenous administration of 1 mg glucagon.

Statistical analysis

Sample size was estimated to be 34 to detect a 4 mmol/mol change in HbA1c in 52 weeks with a power of 95%, alpha 0.05 2-tailed, beta 0.20, standardized effect size 0.7. To take the dropout rate of 30% into account, the aim was to include 45 subjects. IBM SPSS Statistics was used for analysis. Dependent samples Student's *t*-test was used to compare the means of HbA1c level, insulin secretion capacity, BMI, body weight, age, and diabetes duration of the subjects between baseline and 52th week. Person's product-moment correlation test was used to evaluate the relationship between change in HbA1c and insulin secretion capacity or CPI or SUIT. To evaluate cutoff values of diabetes duration, FPG, HbA1c, 0-min CPR, 6-min CPR, delta-CPR, CPI, SUIT, and receiver operating characteristics curve (ROC) analysis were used. Independent sample Student's *t*-test was used to compare the mean of change in HbA1c in 52 weeks between subjects treated with sitagliptin + glimepiride and sitagliptin + gliclazide. Dunnett analysis was used to compare change in HbA1c in 52 weeks among subjects treated with sitagliptin + SUs and sitagliptin + SUs + MET and sitagliptin + SUs + TZD. A p-value of < 0.05 was considered as statistically significant.

Results

Participants

Forty-nine patients were eligible and were consecutively enrolled in the study (◎ **Table 1**). Average age of subjects was 70.0±10.2 years; ratio of male was 60.8%; duration of diabetes was 14.3±8.2 years; average body weight was 62.3±10.4 kg; average BMI was 24.3±3.8 kg/m^2; and HbA1c was 64±9 mmol/mol. All subjects were treated with SUs; 17 subjects (34.7%) were treated with glimepiride (average dose 1.67±1.47 mg) and 32 (65.3%) were treated with gliclazide (average dose 33.8±12.0 mg). Average dosage of basal insulin analogues was 15.0±8.4 units. Glucagon loading test showed that 0-min CPR, 6-min CPR, CPI, and SUIT were 1.65±1.02 ng/ml, 3.37±1.98 ng/ml, 1.19±0.64, and 36.5±22.1, respectively. Sixteen subjects (32.6%) were dropped due to an increase in HbA1c in 8th week; 6 (29.4%) and 11 (34.4%) were dropped in glimepiride- and gliclazide-treated subjects, respectively (◎ **Table 2**). No subjects were dropped for other reasons. Thirty-three subjects completed the study.

HbA1c findings and dosage of SUs and sitagliptin

Therapy adherence was confirmed by certified diabetes educators (nurses) in the study. Adherence of BOT therapy and the switching therapy were almost 100% for both therapies (data not shown).

HbA1c level in 52 weeks in final subjects was significantly decreased from 61±8 to 57±8 mmol/mol ($p<0.01$) (◎ **Table 2**). Change in HbA1c in 52 weeks was −4 mmol/mol (95% CI; −5 to −4 mmol/mol) ($p<0.05$). HbA1c levels in 52 weeks in glimepiride-treated subjects (n=12) were significantly decreased from 63±9 mmol/mol to 55±9 mmol/mol ($p<0.01$). Change in HbA1c in 52 weeks was −8 mmol/mol (95% CI; −11 to −5 mmol/mol) ($p<0.05$). HbA1c levels in 52 weeks in gliclazide-treated subjects (n=21) were significantly decreased from 54±6 to 58±7 mmol/mol ($p<0.05$). Change in HbA1c in 52 weeks was −2 mmol/mol (95% CI; −4 to −0 mmol/mol) ($p<0.05$). There was a significant difference in change in HbA1c in 52 weeks between glimepiride-treated and gliclazide-treated subjects ($p<0.01$). The original dosages of glimepiride and gliclazide before the study were 1.58±0.93 mg/day and 38.2±14.0 mg/day, respectively; the initial dosages at the beginning of the study were significantly decreased to 0.96±0.40 mg/day and 24.8±8.7 mg/day, respectively ($p<0.05$); and the final dosages were significantly increased to 1.42±0.57 mg/day and 31.4±12.0 mg/day, respectively, compared to the initial dosages ($p<0.05$), and were almost equal to the original dosages (◎ **Table 2**). Final dosage of sitagliptin was 74.2±25.4 mg/day in all subjects; 70.8±25.7 mg/day

Subjects (n)	49	**Basal insulin**	15.0±8.4 Units
Age (years)	70.0±10.2	**Medications**	SU 100% Glimepiride 34.7% 1.67±1.47 mg Gliclazide 65.3% 33.8±12.0 mg
Male	60.8%		
Diabetes duration (years)	14.3±8.2		Metformin 22.4% 636±131 mg
Complications	Nephropathy 61.2% Retinopathy 69.4% Neuropathy 42.8% Cardiovascular diseases 34.7%		Thiazolidinedione 16.3% 10.3±3.9 mg α-Glucosidase inhibitors 8.1%
		Glucagon test	1.65±1.02
		0-min CPR (ng/ml)	
		6-min CPR (ng/ml)	3.37±1.98
Weight (kg)	62.3±10.4	Delta CPR (ng/ml)	1.72±1.23
BMI (kg/m^2)	24.3±3.8	**CPI**	1.19±0.64
HbA1c (mmol/mol)	64±8	**SUIT**	36.5±22.1

Table 1 Demographic and clinical features of subjects participating in the study.

Table 2 Changes in HbA1c, and dosages of SUs and sitagliptin in final subjects.

Subjects (n)	Dropout rate (%) (n)	HbA1c level baseline (mmol/mol)	HbA1c level 52nd week (%)	Change in HbA1c (mmol/mol) (95% CI)	Original dosage of SUs (mg)	Initial dosage of SUs (mg)	Final dosage of SUs (mg)	Final dosage of sitagliptin (mg)
Final 33	32.6% 16	61±7	57±7**	−4* (−5 to −4)	–	–	–	74.2±25.4
Glimepiride 12	29.4% 5	63±9	55±9**	−8* (−11 to −5)	1.58±0.93	0.96±0.40*	1.42±0.57*	70.8±25.7
Gliclazide 21	34.4% 11	60±6	58±7*	−2* (−4 to −0)	38.2±14.0	24.8±8.7*	31.4±12.0*	77.3±25.5
SUs 23	30.3% 10	60±7	56±7*	−4* (−6 to −2)	–	–	–	67.4±24.3
SUs+Met 7	36.4% 4	64±9	58±8	−6* (−10 to −2)	–	–	–	87.5±23.1
SUs+TZD 3	62.5% 5	65±6	63±5	−2* (−5 to −0)	–	–	–	100±0.0

*$p<0.05$, **$p<0.01$

in glimepiride-treated subjects; and 77.3±25.5 mg/day in gliclazide-treated subjects with no significant difference between the 2 groups.

Of 33 subjects who completed the study, 22 subjects were treated with sitagliptin and SUs, 6 subjects were treated with sitagliptin and SUs and MET, and 3 subjects were treated with sitagliptin and SUs and TZD; changes in HbA1c in 52 weeks were −4 mmol/mol (95% CI; −6 to −2 mmol/mol) ($p<0.05$), −6 mmol/mol (95% CI; −10 to −2 mmol/mol) ($p<0.05$), and −3 mmol/mol (95% CI; −0.5 to −0 mmol/mol) ($p<0.05$), respectively (◎ **Table 2**). However, there was no significant difference among the 3 groups.

Change in body weight, BMI, and frequency of hypoglycemia

Body weight in final subjects at baseline was 64.2±9.5 kg, and was decreased to 63.5±8.7 kg at 52nd week. Change in body weight in 52 weeks was −0.71 kg (95% CI; −1.42 to −0.004 kg) ($p<0.05$) (◎ **Table 3**). BMI at baseline was 24.8±3.6 kg/m^2, and decreased to 24.5±3.4 kg/m^2 at 52nd week. Change in BMI in 52 weeks was −0.27 kg/m^2 (95% CI; −0.54 to 0.004 kg/m^2) ($p>0.05$). Frequency of hypoglycemia at baseline was 1.21±1.05 times/month, and was significantly decreased to 0.06±0.24 times/month at 52nd week ($p<0.001$). Change in frequency in hypoglycemia in 52 weeks was −1.21 times/months (95% CI; −1.5 to −0.80 times/month) ($p<0.05$) (◎ **Table 3**). During the study, no severe hypoglycemia was noted. During the study, no other adverse events were observed after replacement of basal insulin with sitagliptin.

Differences in HbA1c findings in 8-week in the final and dropped subjects

Sixteen of 49 subjects recruited dropped out after 8 weeks due to increased HbA1c level. The remaining 33 subjects completed the study. HbA1c level at baseline (0-week) in final subjects was 61±8 mmol/mol, and was significantly decreased to

Table 3 Changes in weight, BMI, and frequency in hypoglycemia.

	Weight (kg)	BMI (kg/m^2)	Hypoglycemia (times/month)
0-week	64.2±9.5	24.8±3.6	1.21±1.05
52nd week	63.5±8.7	24.5±3.4	0.06±0.24***
Change (95% CI)	−0.71* (−1.42 to −0.004)	−0.27 (−0.54 to 0.004)	−1.21* (−1.5 to −0.80)

*$p<0.05$, ***$p<0.001$

	Diabetes Duration (Years)	FPG (mM)	HbA1c (mmol/mol)	0-min CPR (ng/ml)	6-min CPR (ng/ml)	Delta CPR (ng/ml)	CPI	SUIT
Cut-off value	16.5	8.2	6.1	1.25	2.80	1.60	1.34	37.5
AUC	0.468	0.507	0.252	0.530	0.570	0.541	0.509	0.482
Specificity	0.600	0.600	0.800	0.800	0.800	0.800	0.600	0.600
Sensitivity	0.545	0.568	0.159	0.432	0.455	0.364	0.545	0.432

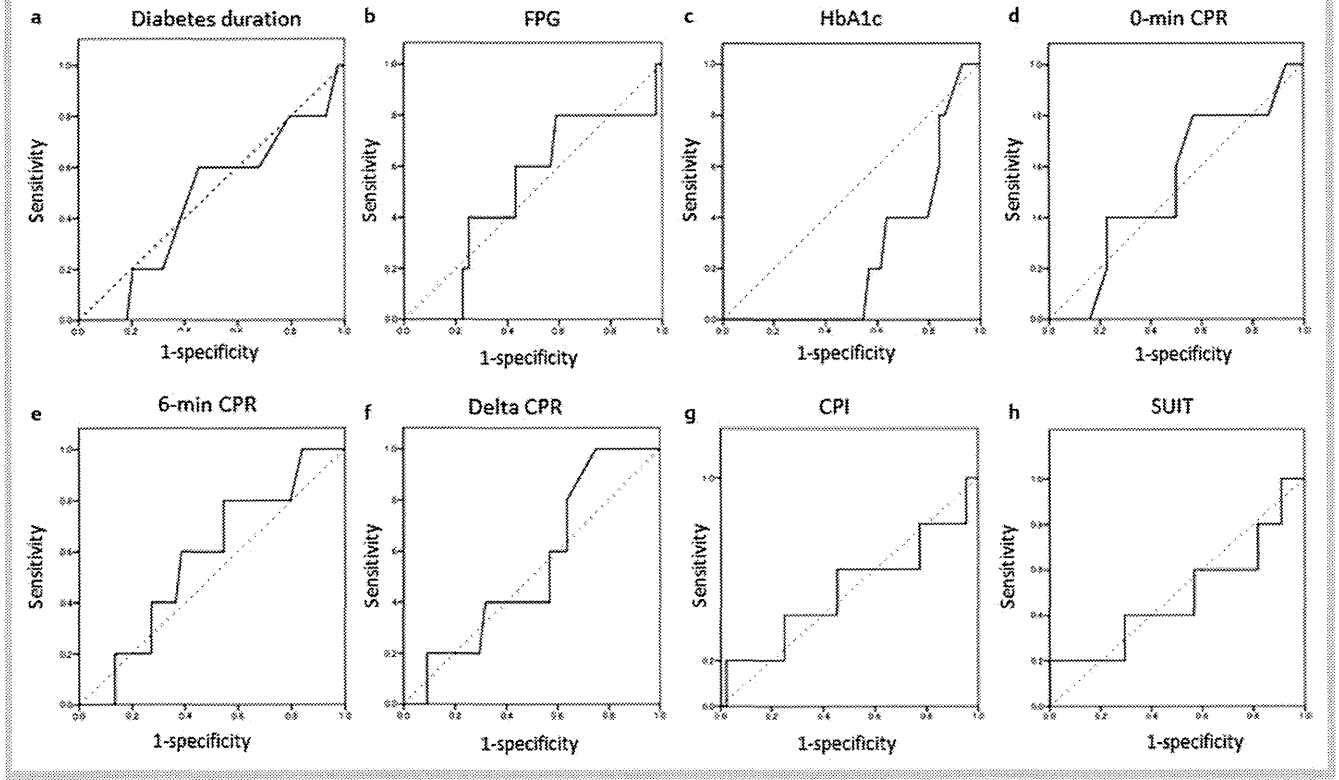

Fig. 1 Cutoff values and receiver-operator characteristic curves of **a** diabetes duration, **b** fasting plasma glucose, **c** HbA1c, **d** 0-min CPR, **e** 6-min CPR, **f** delta CPR, **g** CPI, and **h** SUIT at baseline. CPR: C-peptide reaction; CPI: C-peptide index; SUIT: the secretory unit of islet in transplantation.

Table 4 Changes in HbA1c and background of final and dropped subjects.

	Final subjects	Dropped subjects		Final subjects	Dropped subjects
	33	16		33	16
0 Wk HbA1c (mmol/mol)	61±7	69±10	Original dosage of SUs (mg)	Glimepiride 1.58±0.93 Gliclazide 36.2±10.2	Glimepiride 2.70±2.05 Gliclazide 38.2±14.1
8 Wk HbA1c (mmol/mol)	58±7***	73±10**	Basal insulin (Units)	14.8±9.3	15.2±6.4
Delta HbA1c (mmol/mol) (95% CI)	−4* (−5 to −2)	7* (0.3 to 11)	FPG (mM)	7.4±1.5	8.9±2.9*
Age (years)	69.8±10.7	70.5±9.3	HbA1c (mmol/mol)	61±7	69±10**
Male (%)	66.7	56.3	Glucagon test 0-min CPR (ng/ml)	1.95±1.25	1.37±0.64*
Diabetes duration (years)	12.1±6.6	18.7±9.5*	6-min CPR (ng/ml)	3.81±2.13	2.42±1.21*
Weight (kg)	64.2±9.5	58.4±11.5	Delta CPR (ng/ml)	1.98±1.35	1.16±0.69*
BMI (kg/m²)	24.8±3.6	23.4±4.0	CPI	1.35±0.68	0.92±0.51*
			SUIT	42.7±23.0	23.1±10.6**

*p<0.05, **p<0.01, ***p<0.001

58±7 mmol/mol at 8th week (p<0.001) (◎ **Table 4**). Change in HbA1c was −4 mmol/mol (95% CI; −5 to −2 mmol/mol) (p<0.05). On the other hand, HbA1c level at baseline (0-week) in dropped subjects was significantly higher than that in final subjects (p<0.05), and was significantly increased from 69±9 to 73±11 mmol/mol in 8 weeks (p<0.01). Change in HbA1c was +7 mmol/mol (95% CI; 0.3 to 11 mmol/mol) (p<0.05).

Differences in clinical factors in final and dropped subjects

There were no differences in age, sex, dosage of SUs, or dosage of basal insulin in final and dropped subjects (◎ **Table 4**). Body weight and BMI also were not significantly different (p=0.065 and p=0.2432, respectively). On the other hand, diabetes duration in dropped subjects was longer than that in final subjects (12.1±6.6 vs. 18.7±9.5 years, p<0.05). FPG and HbA1c also were higher in dropped subjects than in final subjects (FPG; 7.4±1.5 vs. 8.9±2.9 mM, p<0.05) (HbA1c; 61±7 vs. 69±9 mmol/mol, p<0.01).

Insulin secretion capacity was significantly higher in final subjects than that in dropped subjects (◎ **Table 4**) (p<0.05). In final subjects, CPR level at 0-min, 6-min, and delta CPR (6-min CPR to 0-min CPR) were 1.95±1.25 ng/ml, 3.81±2.13 ng/ml, and 1.98±1.35 ng/ml, respectively. In dropped subjects, CPR level at 0-min, 6-min, and delta CPR were 1.37±0.64 ng/ml, 2.42±1.21 ng/ml, and 1.16±0.69 ng/ml, respectively. CPI and SUIT index also were significantly higher in final subjects than those in dropped subjects. CPI at baseline in final subjects was 1.35±0.68, while that in dropped subjects was 0.92±0.51 (p<0.05). SUIT at baseline was 42.7±23.0 in final subjects, and 23.1±10.6 in dropped subjects (p<0.01). We examined cutoff values of diabetes duration, FPG, HbA1c, 0-min CPR, 6-min CPR, delta-CPR, CPI, and SUIT by analyzing ROC curves; they were 16.5 years, 8.2 mM, 62 mmol/mol, 1.25 ng/ml, 2.80 ng/ml, 1.60 ng/ml, 1.34, and 37.5, respectively (◎ **Fig. 1**).This indicates that with longer diabetes duration, insulin secretion capacity becomes lower and the consequent poorer glycemic control makes switching BOT-treated patients from basal insulin to sitagliptin unsafe.

Correlation between efficacy of sitagliptin on glycemic control and insulin secretion capacity, CPI, and SUIT

We examined whether or not insulin secretion capacity, CPI, or SUIT at baseline predicted the efficacy of replacing basal insulin with sitagliptin on glycemic control (◎ **Fig. 2**). There was a correlation between change in HbA1c at 8th week and 0-min CPR (r=−0.281), 6-min CPR (r=−0.326), and delta CPR (r=−0.290), assessed by glucagon loading test at baseline (◎ **Fig. 2a, b, c**) (p<0.05). In addition, CPI (r=−0.360) or SUIT (r=−0.306) at baseline was correlated with change in HbA1c at 8th week (◎ **Fig. 2d, e**) (p<0.05). The value of 0-min CPR, 6-min CPR, delta CPR, CPI, and SUIT at which the HbA1c level was not increased by replacement of basal insulin by sitagliptin were calculated to be 1.64 ng/ml, 3.36 ng/ml, 1.71 ng/ml, 1.19, and 36.4, respectively, by Pearson's product-moment correlation test (◎ **Table 5**). The value of 0-min CPR, 6-min CPR, delta CPR, CPI, and SUIT at which the HbA1c level was decreased by 0.5% in 8 weeks were calculated to be 1.86 ng/ml, 3.83 ng/ml, 1.98 ng/ml, 1.36, and 41.3, respectively. Other clinical characteristics of the patients such as disease duration and body weight were not significantly correlated with efficacy of replacing basal insulin with sitagliptin on glycemic control (data not shown).

Discussion

We show here that basal insulin can be switched to sitagliptin with good effects in type 2 diabetes patients treated with BOT. With this treatment, the HbA1c level decreased from 61±7 to 57±7 mmol/mol in 52-week (p<0.01). The change in HbA1c in 52 weeks was −4 mmol/mol (95% CI; −5 to −4 mmol/mol) (p<0.05). The efficacy of switching to sitagliptin from basal insulin was correlated with insulin secretion capacity, CPI, and SUIT; CPI being most correlated marker in the present study. The average CPI in final subjects was 1.35±0.68 ng/ml, while that of dropped subjects was 0.92±0.51 ng/ml. Pearson's product-moment correlation test revealed that HbA1c was improved by switching from basal insulin to sitagliptin if CPI was equal to or higher than 1.19 (◎ **Fig. 2d** and ◎ **Table 5**). Similarly, basal insulin could be switched to sitagliptin if SUIT was equal to or larger than 36.4 (◎ **Fig. 2e** and ◎ **Table 5**). In the dropped subjects, diabetes duration was longer, FPG and HbA1c were worse, 0-min CPR, 6-min CPR, delta-CPR, CPI, and SUIT were lower compared to those in final subjects (◎ **Table 4**). Cutoff values were 16.5 years, 8.2 mM, 62 mmol/mol, 1.25 ng/ml, 2.80 ng/ml, 1.60 ng/ml, 1.34, and 37.5, respectively (◎ **Fig. 1**). This suggests that the efficacy of switching from basal insulin to sitagliptin, when

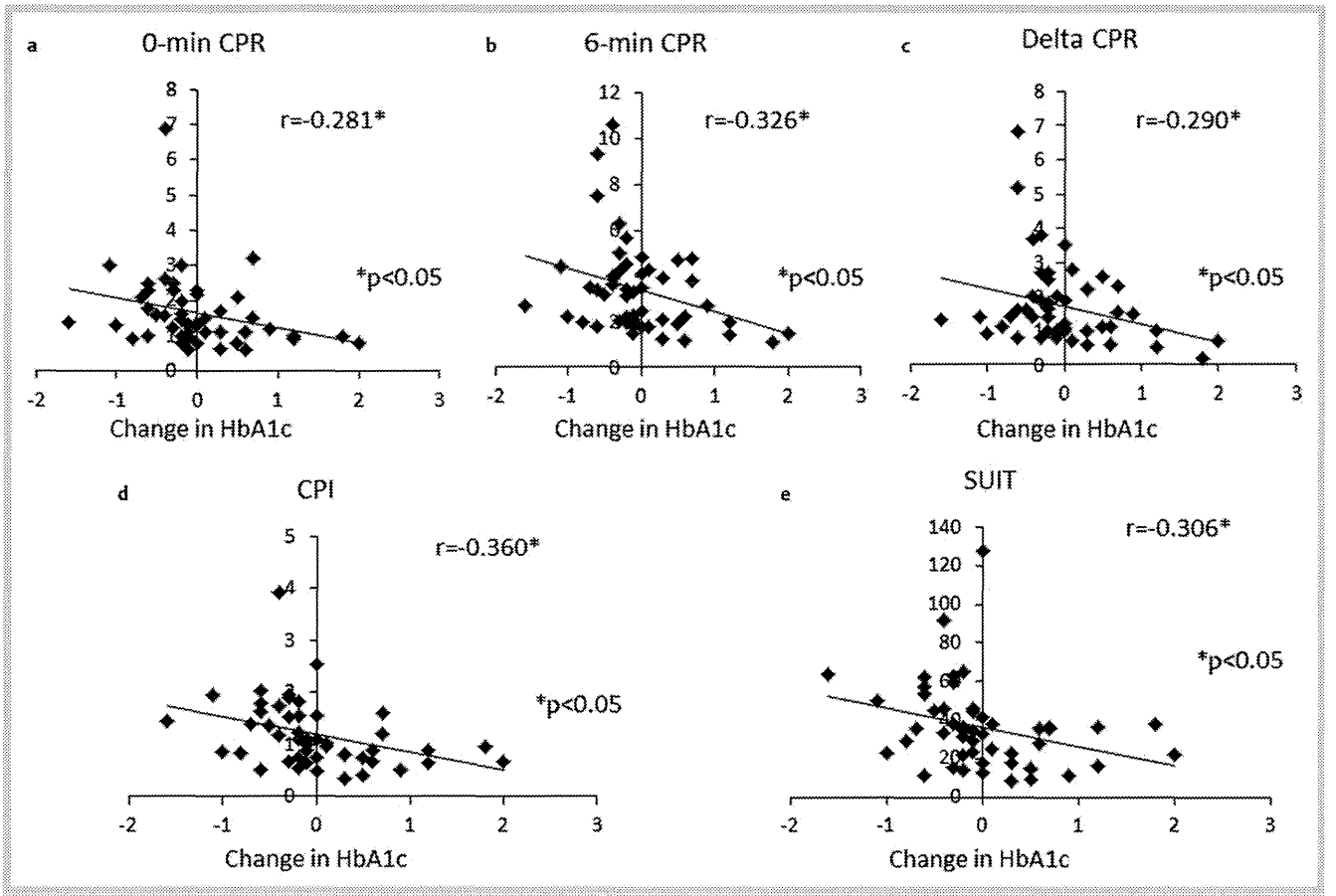

Fig. 2 Relationship between changes in HbA1c in 8 weeks and results of glucagon loading test, CPI, and SUIT at baseline. Changes in HbA1c in 8 weeks and 0-min CPR **a**, 6-min CPR **b**, delta CPR **c**, CPI **d**, and SUIT index **e** at baseline. CPR: C-peptide reaction; CPI: C-peptide index; SUIT: the secretory unit of islet in transplantation. *p<0.05.

Table 5 Correlation between change in HbA1c and insulin secretion capacity.

Change in HbA1c (mmol)	0-Minute CPR (ng/ml)	6-Minute CPR (ng/ml)	Delta CPR (ng/ml)	CPI	SUIT
0.0	1.64	3.36	1.71	1.19	36.4
−5	1.86	3.83	1.98	1.36	41.3

combined with SUs, is dependent on basal glycemic control and the insulin secretion capacity. Baseline HbA1c of dropped subjects was higher than that of the final subjects. A higher dosage of basal insulin was required to reach target HbA1c level in dropped subjects compared to that in final subjects because of lower insulin secretion capacity. Thus, if baseline HbA1c level were reduced by increasing the dosage of basal insulin, it would be difficult to replace basal insulin with sitagliptin.

Replacement of basal insulin by sitagliptin resulted in a reduction in body weight and hypoglycemia. Body weight was reduced by 0.71 kg (95% CI; −1.41 to −0.004 kg) ($p<0.05$). Frequency of hypoglycemia was decreased from 1.21±1.05 to 0.06±0.24 times/month ($p<0.001$). Since sitagliptin is known to be body weight neutral [21,22], discontinuation of basal insulin might contribute to body weight reduction. The combination of basal insulin and SUs often induces mild hypoglycemia by which patients feel a sense of hunger and eat between-meal snacks. This sometimes induces weight gain and poor glycemic control in BOT-treated patients. On the other hand, combination therapy with sitagliptin and low dosage SUs (less than or equal to 2 mg/day glimepiride or 40 mg/day gliclazide) was body weight neutral or led to a decrease in BMI [14]. In the current study, hypoglycemia seldom occurred, and BMI was significantly decreased by 0.38 kg/m^2 (95% CI −0.72 to −0.04 kg/m^2) [14]. Switching from basal insulin to sitagliptin also reduced the frequency of hypoglycemia. Although energy intake was not evaluated between baseline and 52-week in the present study, patients who had previously experienced frequent hypoglycemia reported to their physicians that the number of between-meal snacks in 52 weeks was fewer than at baseline. Thus, excess energy intake may be reduced after switching from basal insulin to sitagliptin to account for some of the body weight reduction and improvement in HbA1c. Another reason for improvement in the HbA1c level may be the reduced postprandial glucose level by the combination therapy with sitagliptin and SUs compared to that by BOT.

The combination therapy of glimepiride and sitagliptin was more effective for HbA1c reduction than that of gliclazide and sitagliptin. Recently, it was reported that cAMP sensor Epac2 is a direct target of several sulfonylureas [23]. Tolbutamide, glibenclimide, and glimepiride bound Epac2 and enhanced glucose-stimulated insulin secretion. However, gliclazide did not bind Epac2. Because Epac2 also mediates the potentiation of insulin secretion by cAMP increased by endogenous incretin, the combination therapy of glimepiride and sitagliptin enhances more insulin secretion through activation of Epac2. This might be a potential mechanism why the combination therapy of glimepir-

ide and sitagliptin was more effective for glycemic control than that of gliclazide and sitagliptin.

Generally, insulin secretion capacity of Japanese is as half as that of Caucasian [16–18]. Therefore, more than 60% of Japanese type 2 diabetes patients are treated with SUs [24]. DPP-4 inhibitor now is one of the most popular OADs, and more than 2 million patients were treated with DPP-4 inhibitors in Japan. Based on pathophysiology of Japanese patients and the mechanism of incretin effect, the combination therapy with SUs and DPP-4 inhibitors seems to be most effective for glycemic control compared to that with other OADs and DPP-4 inhibitors. On the other hand, the main pathophysiology of Caucasian type 2 diabetes is insulin resistance compared to that of Japanese type 2 diabetes [25,26]. Dosage of basal insulin in BOT in Caucasian patients is greater than that in Japanese patients. For example, in 4-T study, the mean dosage of basal insulin was 86 U (1.03 U/kg) [8], while 8.5 U (0.15 U/kg) in Japanese type 2 diabetes [10], and 15 U (0.24 U/kg) in our study. Therefore, it is not sure if basal insulin could be replaced with DPP-4 inhibitors even in subjects treated with high dosage of basal insulin. However, there is still a possibility that in Caucasian subjects whose BMI is less than 25 kg/m^2 and CPI is over 1.3, basal insulin could be replaced with DPP-4 inhibitors. Or, if the combination therapy with high dosage of MET and DPP-4 inhibitors is more effective for glycemic control compared to other combinations in Caucasian type 2 diabetes, basal insulin with MET could be replaced with DPP-4 inhibitors and metformin.

During the course of the disease, type 2 diabetes patients are treated with several OHAs [27,28]. However, if the HbA1c level does not reach less than 53 mmol/mol, insulin treatment is considered the next step [1,2]. BOT is often selected for outpatients because once daily injection is acceptable and the glycemic control is superior, with fewer hypoglycemic episodes and less weight gain compared to biphasic insulin [8]. In Japan, the commonly used SUs are combined with basal insulin in BOT [10]. One of the biggest problems of combination therapy with basal insulin and SUs is the high level of postprandial blood glucose while fasting blood glucose is within normal range. An increase in dosage of SUs or basal insulin does not resolve this problem, and sometimes leads to increased hypoglycemia. However, our results show that better glycemic control and lower frequency of hypoglycemia is obtained when switching from basal insulin to sitagliptin in subjects with sufficiently preserved insulin secretion capacity.

The advantages of discontinuation of basal insulin are 1) patients become free from daily injections; 2) they do not need to regularly perform self-monitoring of blood glucose (SMBG); and 3) oral therapy costs less than insulin therapy.

In summary, basal insulin in BOT can be switched to sitagliptin if CPI and/or SUIT are equal to or higher than 1.19 or 36.4, respectively. On the other hand, sitagliptin can be added to insulin therapy if insulin secretion capacity is not sufficient for switching to sitagliptin. However, the effectiveness of combination therapy with basal insulin and sitagliptin on glycemic control in type 2 patients with CPI and/or SUIT less than 1.19 or 36.4, respectively, is unknown. Further studies are required to determine the optimum insulin secretion capacities for switching BOT therapy to sitagliptin combined with SUs or combination therapy with sitagliptin and basal insulin or GLP-1 receptor analogues.

Acknowledgements

The study conception and protocol were by SH and NI. Patient examinations were by SH, TF, TK, and MA. Collection of data was by YW and MO. The statistical analysis was by DT, SY, and YF. The manuscript development was by Dr. SH and NI.

Conflict of Interest

None of the authors have any conflicts of interest to declare.

References

1 *Nathan DM, Buse JB, Davidson MB, Ferrannini E, Holman RR, Sherwin R, Zinman B; American Diabetes Association; European Association for Study of Diabetes.* Medical management of hyperglycemia in type 2 diabetes: a consensus algorithm for the initiation and adjustment of therapy: a consensus statement of the American Diabetes Association and the European Association for the Study of Diabetes. Diabetes Care 2009; 32: 193–203

2 *Nathan DM, Buse JB, Davidson MB, Ferrannini E, Holman RR, Sherwin R, Zinman B; American Diabetes Association; European Association for Study of Diabetes.* Medical management of hyperglycemia in type 2 diabetes mellitus: a consensus algorithm for the initiation and adjustment of therapy: a consensus statement from the American Diabetes Association and the European Association for the Study of Diabetes. Diabetologia 2009; 52: 17–30

3 *Heinemann L, Linkeschova R, Rave K, Hompesch B, Sedlak M, Heise T.* Time-action profile of the long-acting insulin analog insulin glargine (HOE901) in comparison with those of NPH insulin and placebo. Diabetes Care 2000; 23: 644–649

4 *Plank J, Bodenlenz M, Sinner F, Magnes C, Görzer E, Regittnig W, Endahl LA, Draeger E, Zdravkovic M, Pieber TR.* A double-blind, randomized, dose-response study investigating the pharmacodynamic and pharmacokinetic properties of the long-acting insulin analog detemir. Diabetes Care 2005; 28: 1107–1112

5 *Swinnen SG, Simon AC, Holleman F, Hoekstra JB, Devries JH.* Insulin detemir versus insulin glargine for type 2 diabetes mellitus. Cochrane Database Syst Rev 2011; 6: CD006383

6 *Blicklé JF, Hancu N, Piletic M, Profozic V, Shestakova M, Dain MP, Jacqueminet S, Grimaldi A.* Insulin glargine provides greater improvements in glycaemic control vs. intensifying lifestyle management for people with type 2 diabetes treated with OADs and 7–8% A1c levels. The TULIP study. Diabetes Obes Metab 2009; 11: 379–386

7 *Schreiber SA, Ferlinz K, Haak T.* The long-term efficacy of insulin glargine plus oral antidiabetic agents in a 32-month observational study of everyday clinical practice. Diabetes Technol Ther 2008; 10: 121–127

8 *Holman RR, Farmer AJ, Davies MJ, Levy JC, Darbyshire JL, Keenan JF, Paul SK; 4-T Study Group.* Three-year efficacy of complex insulin regimens in type 2 diabetes. N Engl J Med 2009; 361: 1736–1747

9 *Pfohl M, Dippel FW, Kostev K, Fuchs S, Kotowa W.* Different persistence on initial basal supported oral therapy in Type 2 diabetics is associated with unequal distributions of insulin treatment regimens under real-life conditions in Germany. Int J Clin Pharmacol Ther 2010; 48: 761–766

10 *Kadowaki T.* Analysis of ALOHA (add-on Lantus® to OHA) study: Basal supported oral therapy (BOT) with insulin glargine resulted in reduction of HbA1c, FPG and PPG with nearly 2% incidence of adverse drug reactions. Dubai: World Diabetes Congress, 2011

11 *Seino Y, Fukushima M, Yabe D.* GIP and GLP-1, two incretin hormones: Similarities and differences. J Diabetes Invest 2010; 1: 8–23

12 *Tajima N, Kadowaki T, Odawara M, Nishi M, Taniguchi T, Arjona Ferreira JC.* Addition of sitagliptin to ongoing glimepiride therapy in Japanese patients with type 2 diabetes over 52 weeks leads to improved glycemic control. Diabetol Int 2011; 2: 32–44

13 *Hermansen K, Kipnes M, Luo E, Fanurik D, Khatami H, Stein P.* Efficacy and safety of the dipeptidyl peptidase-4 inhibitor, sitagliptin, in patients with type 2 diabetes mellitus inadequately controlled on glimepiride alone or on glimepiride and metformin. Diabetes Obes Metab 2007; 9: 733–745

14 *Harashima SI, Ogura M, Tanaka D, Fukushima T, Wang Y, Koizumi T, Aono M, Murata Y, Seike M, Inagaki N.* Sitagliptin add-on to low dosage sulfonylureas: efficacy and safety of combination therapy on glycemic control and insulin secretion capacity in type 2 diabetes. Int J Clin Prac 2012; 66: 465–476
15 *Kubota A, Matsuba I, Saito T, Nabe K, Seino Y.* Secretory units of islets in transplantation index is a useful clinical marker to evaluate the efficacy of sitagliptin in treatment of type 2 diabetes mellitus. J Diabetes Invest 2011; 5: 377–380
16 *Fukushima M, Usami M, Ikeda M, Nakai Y, Taniguchi A, Matsuura T, Suzuki H, Kurose T, Yamada Y, Seino Y.* Insulin secretion and insulin sensitivity at different stages of glucose tolerance: a cross-sectional study of Japanese type 2 diabetes. Metabolism 2004; 53: 831–835
17 *Fukushima M, Suzuki H, Seino Y.* Insulin secretion capacity in the development from normal glucose tolerance to type 2 diabetes. Diabetes Res Clin Pract 2004; 66: S37–S47
18 *Abdul-Ghani MA, Matsuda M, Jani R, Jenkinson CP, Coletta DK, Kaku K, DeFronzo RA.* The relationship between fasting hyperglycemia and insulin secretion subjects with normal or impaired glucose tolerance. Am J Physiol Endocrinol Metab 2008; 295: E401–E406
19 *Funakoshi S, Fujimoto S, Hamasaki A, Fujiwara H, Fujita Y, Ikeda K, Hamamoto Y, Hosokawa M, Seino Y, Inagaki N.* Analysis of factors influencing pancreatic beta-cell function in Japanese patients with type 2 diabetes: Association with body mass index and duration of diabetic exposure. Diabetes Res Clin Pract 2008; 82: 353–358
20 *Yamada Y, Fukuda K, Fujimoto S, Hosokawa M, Tsukiyama K, Nagashima K, Fukushima M, Suzuki H, Toyoda K, Sassa M, Funakoshi S, Inagaki N, Taniguchi A, Sato TS, Matsumoto S, Tanaka K, Seino Y.* SUIT, secretory units of islets in transplantation: An index for therapeutic management of islet transplanted patients and its application to type 2 diabetes. Diabetes Res Clin Pract 2006; 74: 222–226
21 *Esposito K, Cozzolino D, Bellastella G, Maiorino MI, Chiodini P, Ceriello A, Giugliano D.* Dipeptidyl peptidase-4 inhibitors and HbA1c target of <7% in type 2 diabetes: meta-analysis of randomized controlled trials. Diabetes Obes Metab 2011; 13: 594–603
22 *Gallwitz B, Häring HU.* Future perspectives for insulinotropic agents in the treatment of type 2 diabetes-DPP-4 inhibitors and sulphonylureas. Diabetes Obes Metab 2010; 12: 1–11
23 *Zhang CL, Katoh M, Shibasaki T, Minami K, Sunaga Y, Takahashi T, Yokoi N, Iwasaki M, Miki T, Seino S.* The cAMP sensor Rpac2 is a direct target of antidiabetic sulfonylurea drugs. Science 2009; 25: 607–610
24 *Arai K, Matoba K, Hirao K, Matsuba I, Takai M, Takeda H, Kanamori A, Yamauchi M, Mori H, Terauchi Y.* Present status of sulfonylurea treatment for type 2 diabetes in Japan: second report of a cross-sectional survey of 15652 patients. Endocr J 2010; 57: 499–507
25 *Welch S, Gebhart SS, Bergman RN, Phillips LS.* Minimal model analysis of intravenous glucose tolerance test-derived insulin sensitivity in diabetic subjects. J Clin Endocrinol Metab 1990; 71: 1508–1518
26 *Taniguchi A, Nakai Y, Fukushima M, Kawamura H, Imura H, Nagata I, Tokuyama K.* Pathogenic factors responsible for glucose intolerance in patients with NIDDM. Diabetes 1992; 41: 1540–1546
27 *Tahrani AA, Bailey CJ, Del Prato S, Barnett AH.* Management of type 2 diabetes: new and future developments in treatment. Lancet 2011; 378: 182–197
28 *DeFronzo RA.* Current issues in the treatment of type 2 diabetes. Overview of newer agents: where treatment is going. Am J Med 2010; 123: S38–S48

DIABETES/METABOLISM RESEARCH AND REVIEWS
Diabetes Metab Res Rev 2013; **29**: 77–84.
Published online in Wiley Online Library (wileyonlinelibrary.com) **DOI:** 10.1002/dmrr.2363

RESEARCH ARTICLE

Self-monitoring of blood glucose (SMBG) improves glycaemic control in oral hypoglycaemic agent (OHA)-treated type 2 diabetes (SMBG-OHA study)

Shin-ichi Harashima[1]*
Toru Fukushima[1]
Mayumi Sasaki[1]
Yuichi Nishi[1]
Shimpei Fujimoto[1]
Masahito Ogura[1]
Shunsuke Yamane[1]
Daisuke Tanaka[1]
Norio Harada[1]
Akihiro Hamasaki[1]
Kazuaki Nagashima[1]
Yuko Nakahigashi[1]
Yutaka Seino[2]
Nobuya Inagaki[1]

[1]*Department of Diabetes and Clinical Nutrition, Graduate School of Medicine, Kyoto University, Kyoto, Japan*

[2]*Department of Diabetes and Clinical Nutrition Kansai Electric Power Hospital, Osaka, Japan*

*Correspondence to: Shin-ichi Harashima, Department of Diabetes and Clinical Nutrition, Graduate School of Medicine, Kyoto University, Kyoto 606-8507, Japan.
E-mail: harasima@metab.kuhp.kyoto-u.ac.jp

Received: 23 February 2012
Revised: 8 August 2012
Accepted: 25 August 2012

Abstract

Background We conducted a clinical research study to determine the effect of self-monitoring of blood glucose (SMBG) on glycaemic control and the value of a putatively less painful blood sampling technique on SMBG in oral hypoglycaemic agent-treated type 2 diabetes patients; SMBG has not been broadly applied in non-insulin-treated patients in Japan.

Methods One hundred thirty-seven subjects were recruited for the 24-week, prospective, comparison study and randomized into three groups: 46, no SMBG group; 46, fingertip group; and 45, palm group. The primary endpoint was change in HbA_{1c}. The secondary endpoints were SMBG compliance, dropout rate, treatment changes, and patient's and physician's satisfaction.

Results Six subjects in the fingertip group (13.2%) and one subject in the palm group (2.2%) were dropped because of pain. A_{1C} level of all subjects at 24-week was decreased more in the fingertip (−0.23%) and palm (−0.16%) groups than that in the no SMBG group (+0.31%) ($p < 0.05$). SMBG compliance was higher in the fingertip group (2.17 times/day) than that in the palm group (1.65 times/day) ($p < 0.05$). A_{1C} level of treatment-unchanged subjects was decreased more in the fingertip (−0.25%) and palm (−0.21%) groups than that in the no SMBG group (+0.30%) ($p < 0.05$). SMBG compliance was higher in the fingertip group (2.24 times/day) than that in the palm group (1.65 times/day) ($p < 0.05$). Patient's questionnaire showed that 84.1% of the fingertip group and 90.2% of the palm group were satisfied with SMBG. Physician's satisfaction was higher in the palm group (94.0%) than that in the fingertip group (80.0%) ($p < 0.05$).

Conclusion SMBG is beneficial for glycaemic control, and palm blood sampling is a useful procedure for oral hypoglycaemic agent-treated type 2 diabetes.

Keywords type 2 diabetes; palm puncture; self-monitoring of blood glucose (SMBG)

Introduction

Self-monitoring of blood glucose (SMBG) is a tool for patients with diabetes to detect patterns of blood glucose control. Results of SMBG can be useful to make adjustments in diet, physical activity, and medications in order to achieve glycaemic targets, preventing hypoglycaemic events. In addition, it has been reported that SMBG is associated with decreased diabetes-related morbidity and all-cause mortality in insulin-treated patients as well as in insulin-naïve